Stem Cell Reports
Resource
ISSCR
OPEN ACCESS

Robotic high-throughput biomanufacturing and functional differentiation of human pluripotent stem cells

Carlos A. Tristan,[1] Pinar Ormanoglu,[1] Jaroslav Slamecka,[1] Claire Malley,[1] Pei-Hsuan Chu,[1] Vukasin M. Jovanovic,[1] Yeliz Gedik,[1] Yogita Jethmalani,[1] Charles Bonney,[1] Elena Barnaeva,[1] John Braisted,[1] Sunil K. Mallanna,[1] Dorjbal Dorjsuren,[1] Michael J. Iannotti,[1] Ty C. Voss,[1] Sam Michael,[1] Anton Simeonov,[1] and Ilyas Singeç[1,*]

[1]National Center for Advancing Translational Sciences (NCATS), Division of Preclinical Innovation (DPI), Stem Cell Translation Laboratory (SCTL), National Institutes of Health (NIH), 9800 Medical Center Drive, Rockville, MD 20850, USA

*Correspondence: ilyas.singec@nih.gov

https://doi.org/10.1016/j.stemcr.2021.11.004

SUMMARY

Efficient translation of human induced pluripotent stem cells (hiPSCs) requires scalable cell manufacturing strategies for optimal self-renewal and functional differentiation. Traditional manual cell culture is variable and labor intensive, posing challenges for high-throughput applications. Here, we established a robotic platform and automated all essential steps of hiPSC culture and differentiation under chemically defined conditions. This approach allowed rapid and standardized manufacturing of billions of hiPSCs that can be produced in parallel from up to 90 different patient- and disease-specific cell lines. Moreover, we established automated multi-lineage differentiation and generated functional neurons, cardiomyocytes, and hepatocytes. To validate our approach, we compared robotic and manual cell culture operations and performed comprehensive molecular and cellular characterizations (e.g., single-cell transcriptomics, mass cytometry, metabolism, electrophysiology) to benchmark industrial-scale cell culture operations toward building an integrated platform for efficient cell manufacturing for disease modeling, drug screening, and cell therapy.

INTRODUCTION

Human pluripotent stem cells (hPSCs) are characterized by extensive self-renewal capacity and differentiation into all somatic cell types, enabling novel approaches to model, diagnose, and treat human diseases (Kimbrel and Lanza, 2020; Sato et al., 2019; Sharma et al., 2020). However, several important challenges remain to be addressed for their efficient and safe utilization. These challenges include technical and biological variability, lack of standardization, laborious differentiation protocols, limited methods for scale up, and inefficient manufacturing of functional cell types representing the diversity of human tissues. Since isolation of the first human embryonic stem cells (hESCs) (Thomson et al., 1998), significant progress has been made in improving cell culture conditions, including the development of new reagents, coating substrates, medium formulations, and passaging tools (Chen et al., 2011; Kuo et al., 2020; Ludwig et al., 2006; Rodin et al., 2014). Despite these advances, manual cell culture of hPSCs remains time consuming, laborious, and subject to human bias or error (e.g., risk of contamination, medium change at different intervals). Other inherent challenges are due to variability in handling cells and reagents across laboratories, use of different reprogramming methods, and cell-line-to-cell-line variability (Cahan and Daley, 2013; Niepel et al., 2019; Osafune et al., 2008; Panopoulos et al., 2017).

Automated cell culture has several practical and scientific characteristics designed to improve quality control, increase productivity, implement standard operating procedures (SOPs), and develop commercial cellular products (Aijaz et al., 2018; Daniszewski et al., 2018). These advantages ensure scale-up of cell manufacturing, standardization of liquid handling, control of incubation times, minimization of batch-to-batch variability, reduction of human error, and seamless documentation of operations. Automated cell reprogramming by using liquid handlers can increase efficiency and reproducibility of new induced pluripotent stem cell (iPSC) line generation (Paull et al., 2015). Previous studies used various two- and three-dimensional (2D, 3D) systems to either automate or scale-up some aspects of hPSC culture (Archibald et al., 2016; Hookway et al., 2016; Konagaya et al., 2015; Liu et al., 2014; McLaren et al., 2013; Rigamonti et al., 2016; Schwedhelm et al., 2019; Soares et al., 2014a; Thomas et al., 2009). However, a comprehensive automation strategy for biomanufacturing of hPSCs under flexible scale-up and scale-down conditions and compatibility with 2D and 3D culture (e.g., embryoid bodies, neurospheres, monolayer differentiation) has not been established so far. Here we present and characterize a versatile robotic cell culture platform that can be utilized for scale-up and multi-lineage differentiation of human induced pluripotent stem cells (hiPSCs). We performed a functional analysis of neurons, cardiomyocytes, and hepatocytes and demonstrate their utility for high-throughput screening and Zika virus experiments. We envision that automation will help to overcome technical and economic challenges and leverage the full translational potential of hiPSCs.

RESULTS

Automated and scalable culture of hPSCs

The CompacT SelecT (CTST) platform is a modular robotic system that integrates a full range of cell culture procedures under sterile conditions that mimic the manual cell culture process (Figure 1). These procedures include automated handling of different cell culture vessels, pipetting large and small volumes at adjustable speeds, cell counting, cell viability analysis, cell density assessment, microscopic imaging, cell passaging, cell harvest, and medium changes. Moreover, two independent incubator carousels (humidified 37°C, 5% CO_2) enable culturing cells in various cell culture vessels (T75 and T175 flasks and 6-, 24-, 96-, or 384-well formats). Notably, the CTST system has the capacity to simultaneously culture up to 280 assay-ready plates and up to 90 different hiPSC lines in large T175 flasks (Figures 1 and 2A, Video S1, and full movie: https://youtu.be/-GSsTSO-WCM). Moreover, as CTST is handling different cell lines and protocols, scientists may remotely access, control, and monitor ongoing experiments without the need to physically enter the laboratory. Hence, the system allows non-stop cell culture operations with minimal manual intervention.

To establish standardized high-throughput protocols for CTST, we focused on culturing hPSCs under feeder-free conditions using Essential 8 (E8) medium, recombinant vitronectin (VTN-N) as coating substrate, and EDTA for cell passaging. Use of EDTA for non-enzymatic cell dissociation was critical to minimize cellular stress and skip a manual intervention step (offline centrifugation and removal of enzymatic cell dissociation reagents). Under these chemically defined conditions, we were able to robustly culture, expand, and cryopreserve various hESC and hiPSC lines over the last 5 years (Figure S1A and Table S1). hPSCs maintained typical characteristics, such as growth in densely packed colonies, high nucleus-to-cytoplasm ratio, expression of pluripotency-associated markers OCT4 and NANOG, and normal karyotypes (Figures 2B–2E and S2A–S2C). Energy production in hPSCs depends on high glycolytic rates (Gu et al., 2016; Zhang et al., 2016), and live-cell metabolic analysis (Seahorse XF analyzer) confirmed expected metabolic profiles in hESCs and hiPSCs when cultured manually or robotically (Figures 2F, 2G, S2D, and S2E).

Because suboptimal conditions such as overgrowing cells in high-cell-density cultures can lead to cellular stress and impaired quality of hPSCs (Horiguchi et al., 2018; Jacobs et al., 2016; Paull et al., 2015), we sought to directly compare manual with automated cell cultures. Medium change intervals can be precisely controlled and documented by CTST, whereas manual cell culture is typically investigator dependent and variable. To monitor manual cell culture, we maintained hPSCs in live-cell imaging systems (IncuCyte), which enable the monitoring of cell growth and daily interventions by investigators. By tracking the online use of our IncuCyte instruments, we were able to capture the typical variability of medium change intervals in our laboratory (Figure 2H), which is likely to be representative for most laboratories culturing hPSCs. In contrast, medium change intervals were tightly controlled by using CTST (Figure 2H). To assess the consequences of variable medium change intervals, we measured the spent media of cultures maintained either manually or robotically. Indeed, culturing hPSCs by CTST resulted in less deviation from the mean in several measured endpoints such as oxygen concentration, pH fluctuations, lactate levels, glucose concentration, and ionic milieu (calcium, sodium, potassium) (Figures 2I–2O and S2F–S2L).

Process automation is of particular importance to produce large quantities of cells in a standardized fashion for high-throughput applications. One additional challenge for cell manufacturing is the fact that hPSCs are sensitive to environmental perturbations, and poor cell survival can be a limiting factor (Archibald et al., 2016; Soares et al., 2014a; Watanabe et al., 2007). Taking advantage of the newly developed CEPT small molecule, which promotes viability and cytoprotection during routine cell passaging (Chen et al., 2021), we aimed at optimizing the expansion of hPSCs. Combining CTST with the CEPT cocktail enabled consistent cell passaging and cell growth (Figures 2P and S2M). Robotic cell passaging was robust and predictable, resulting in minimal cell death, and cultures were devoid of cellular debris at 24 h post-passaging in the presence of CEPT (Figure S1B). The efficiency of this approach enabled rapid scale-up and production of large quantities of hPSCs. For instance, using the WA09 cell line and starting with one T175 flask containing 5.25 million cells and passaging at 70% to 80% confluency (~42 million cells per flask) in a 1:6 ratio every 3 days, we were able to generate a total of 9.07 billion hPSCs in 12 days (Figure 2Q). To our knowledge, such dramatic scale-up in a short period of time has not been reported previously and should be invaluable for biobanking of hPSCs or CryoPause, an approach to increase experimental reproducibility by using the same batch of cryopreserved cells (Wong et al., 2017). Furthermore, since CTST can operate in a virtually non-stop fashion and handle large flasks or assay-ready plates, we compared these features with typical manual cell culture performed during a typical 8 h workday. This comparison demonstrated enormous advantages of robotic cell culture for biomanufacturing large quantities of pluripotent and differentiated cells (Table S2).

Similar molecular signatures of hPSCs cultured manually or robotically

Manual cell culture is the most widely used approach in the stem cell field. In parallel to our automated platform and

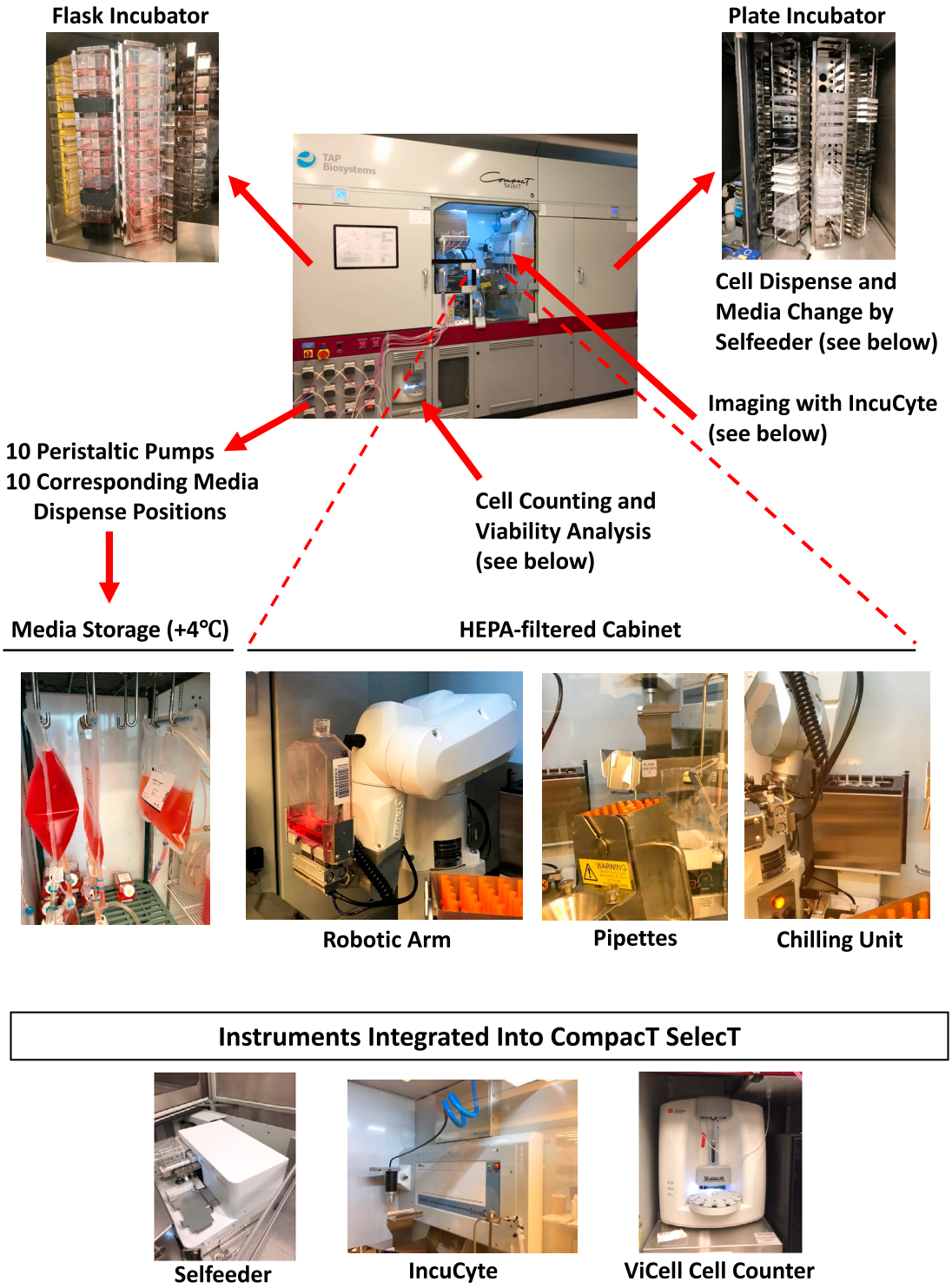

Figure 1. Overview of the automated CTST system

Features and components of CTST, including flask incubator, plate incubator, storage of large volumes of medium, cell counting, viability analysis, microscopic imaging, and a sterile HEPA-filtered cabinet housing a robotic arm, various pipettes, and a chilling unit to store temperature-sensitive reagents such as recombinant proteins.

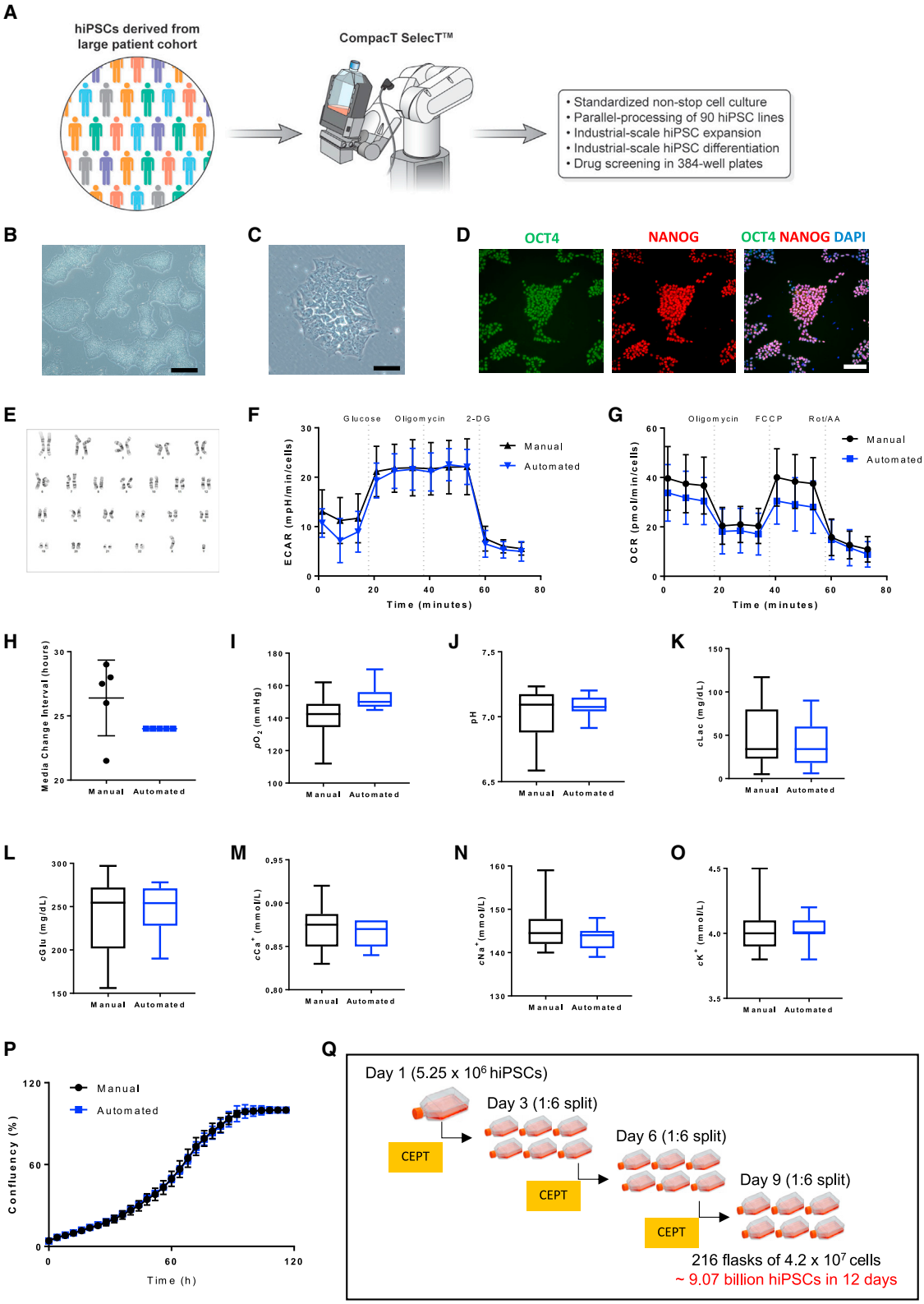

(legend on next page)

depending on experimental needs, we continue to carry out significant amounts of cell culture work manually. To perform a side-by-side comparison of cultures maintained manually versus robotically, we performed a single-cell analysis, including RNA sequencing (RNA-seq) and mass cytometry. Deriving detailed information at single-cell resolution can aid in defining cell type identities and cellular heterogeneity (Quadrato et al., 2017; Veres et al., 2019). We randomly selected hESCs (WA09) and hiPSCs (LiPSC-GR1.1) that were cultured either manually or robotically by different investigators in our laboratory, and samples were processed for RNA-seq using the 10× Genomics platform. Single-cell transcriptome libraries of 18,817 cells derived from manual (5,573 cells for WA09; 4,835 cells for LiPSC-GR1.1) and automated (4,485 cells for WA09; 3,922 cells for LiPSC-GR1.1) cultures were analyzed for differential gene expression and comparison between both culture conditions. t-Distributed stochastic neighbor embedding (t-SNE) projection demonstrated that hiPSCs and hESCs cultured either manually or robotically showed a highly similar distribution (Figures 3A–3D). Thus, cells cultured by CTST substantially mirrored manually cultured hESCs and hiPSCs. Of 32,894 transcripts analyzed, there were only 98 differentially expressed genes among manually and robotically cultured hiPSCs (Figure 3B and Table S3). Similarly, there were only 15 differentially expressed genes in the hESC line (Figure 3D and Table S3). A total of only five genes (*SFRP1*, *SLIRP*, *HNRNPAB*, *APOE*, and *COPS9*) were downregulated comparing automated with manual cell cultures (Figure 3D and Table S3). Together, it was striking to see that the transcriptomic profiles of manually and robotically cultured cells were largely overlapping (Figure 3E).

Cytometry time-of-flight (CyTOF) is a new technology that allows the simultaneous analysis of more than 30 proteins in single cells by using metal-conjugated antibodies (Qin et al., 2020; Zunder et al., 2015). We used a panel of 25 cell-surface cluster-of-differentiation (CD) antigens and intracellular proteins, including phosphorylated proteins (Table S4), to carefully compare markers of cell health and pluripotency in hPSCs cultured either manually or robotically. The expression of pluripotency-associated transcription factors OCT4, NANOG, and SOX2 showed, again, strikingly similar expression levels across different samples (Figures 4A–4C). A total of 96,861 cells derived from manual (11,898 cells from WA09; 19,217 cells from LiPSC-GR1.1) and automated (32,889 hESCs; 32,857 hiPSCs) cell culture experiments were subjected to single-cell mass cytometry. An analysis of an additional 22 proteins covering diverse cellular mechanisms confirmed the predominant similarity of cultures maintained either manually or by automation (Figures 4B and 4C). Expression of the cell-surface marker and sialoglycoprotein CD24 is regulated during cell reprogramming, and its expression may indicate a more differentiated state compared with naive pluripotency (Shakiba et al., 2015). The hiPSC line displayed a population of cells (cluster 6) that lacked CD24 expression and could be distinguished from the main cluster (cluster 3, Figure 4B). Interestingly, cluster 6 cells were more abundant in manually cultured hiPSC samples (Figure 4B). However, the hESC line (WA09) showed only a negligible percentage of CD24-negative cells in both automated and manual cell culture (Figure 4C).

Automated embryoid body formation

Cell differentiation is a dynamic process with cells progressing through developmental states, which can be recapitulated *in vitro* by spontaneous or controlled differentiation when appropriate factors and morphogens are administered at defined time points. Spontaneous differentiation of hPSCs by embryoid body (EB) formation is a widely used assay for pluripotency assessment (i.e., capacity to differentiate into ectoderm, mesoderm, and

Figure 2. Characterization of hiPSCs (LiPSC-GR1.1) cultured by CTST

(A) Characteristics and advantages of automated cell culture.

(B) Representative hiPSCs growing in densely packed colonies at 3 days post-passaging. Scale bar, 500 μm.

(C) Colony of hiPSCs showing typical morphological features of human pluripotent cells at 3 days post-passaging. Scale bar, 250 μm.

(D) hiPSCs immunostained for pluripotency-associated markers OCT4 and NANOG. Scale bar, 100 μm.

(E) Long-term robotically cultured hiPSCs maintain a normal karyotype (passage 40).

(F) Seahorse XF glycolysis stress test profile comparison of glycolytic function in hiPSCs maintained by automated or manual cell culture. Cells were treated with serial injections of metabolic modulators (glucose, oligomycin, 2-deoxyglucose [2-DG]).

(G) Seahorse XF mitochondrial stress test profile comparison of mitochondrial function in hiPSCs maintained by automated or manual cell culture. Cells were treated with serial injections of metabolic modulators (oligomycin, FCCP, and rotenone/antimycin A [Rot/AA]).

(H) Comparison of medium change intervals during automated and manual cell culture of hiPSCs.

(I–O) Supernatants of cultures maintained manually or robotically were measured daily (Vi-Cell MetaFLEX Bioanalyte Analyzer). Boxplots show the variation of spent medium from hiPSC cultures. (I) pO_2, (J) pH, (K) cLac, (L) cGlu, (M) cCa^+, (N) cNa^+, (O) cK^+.

(P) Image-based analysis comparing cell growth in hiPSC cultures expanded manually and robotically.

(Q) Automated cell expansion strategy showing massive scale-up in only 12 days. Data expressed as mean ± SD, n > 3 biological replicates using two independent cell lines (B–P). p = 0.0001 in (I), unpaired *t* test.

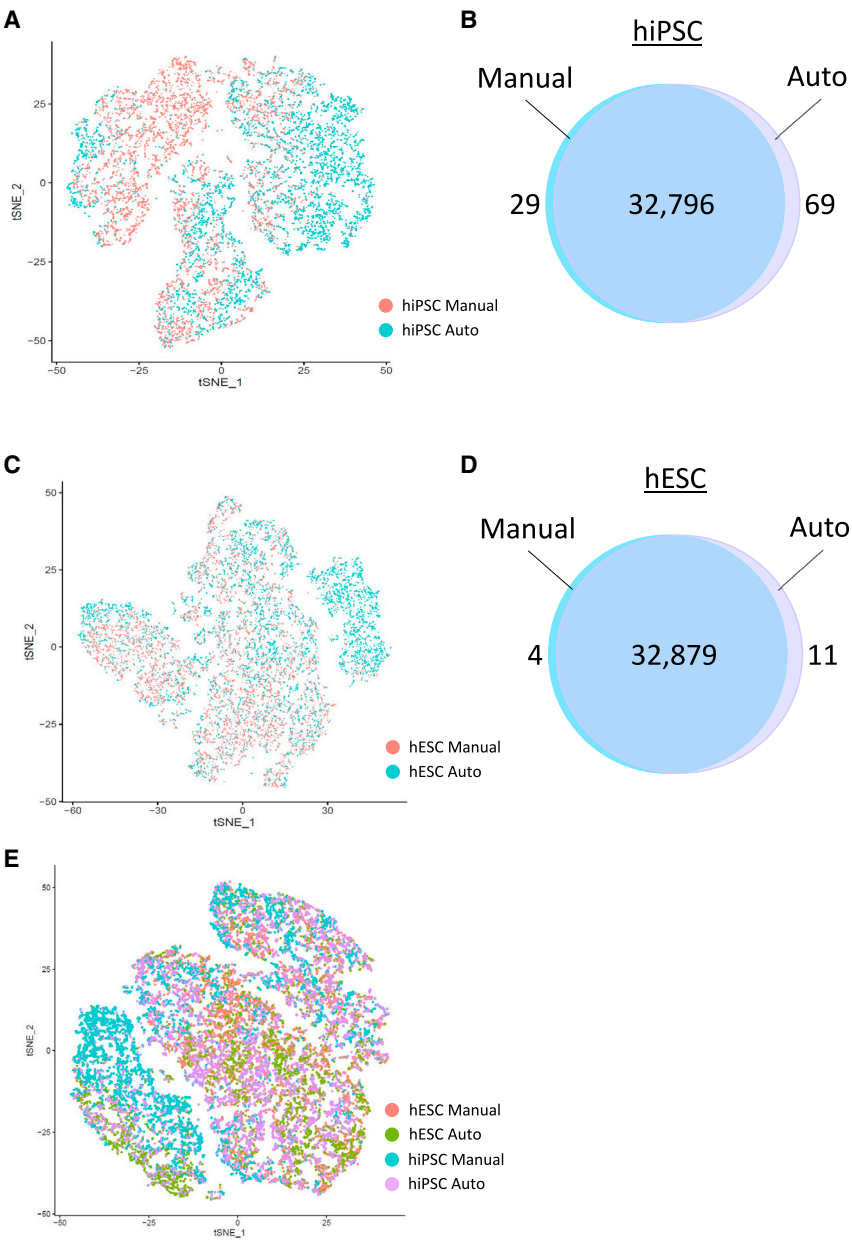

Figure 3. Single-cell RNA-seq and comparison of manual and automated cell culture

(A and C) t-SNE plots illustrating (A) hiPSCs (LiPSC-GR1.1) and (C) hESCs (WA09) maintained either manually or robotically show a high degree of transcriptomic similarity.

(B and D) Venn diagrams showing overlap of expressed genes in (B) hiPSCs (LiPSC GR1.1) and (D) hESCs (WA09).

(E) Direct comparison of transcriptomes of hiPSCs (LiPSC-GR1.1) and hESCs (WA09) cultured manually and robotically. Data from n = 5,573, 4,835, 4,485, and 3,922 single cells obtained from n = 4 independent experiments using two independent cell lines for hESC manual, hiPSC manual, hESC auto, and hiPSC auto, respectively (A–E). Single-cell RNA-seq data were analyzed in the Seurat R package.

endoderm), toxicity testing, organoid formation, and other developmental studies (Guo et al., 2019; Lancaster et al., 2013; Osafune et al., 2008; Tsankov et al., 2015). Hence, developing defined protocols for automated large-scale production of EBs is of great relevance. Typically, in manual cell culture work EBs are maintained as free-floating 3D structures in ultra-low attachment six-well plates. Although the CTST system can culture cells and change medium in different plate formats (6, 24, 96, or 384 wells), T175 flasks would represent the largest vessel for EB production in this context. To our knowledge, T175 flasks are currently not available in an ultra-low attachment version. However, we found that rinsing regular T175 flasks with a commercially available anti-adherence solution (STEMCELL Technologies) was sufficient to prevent unwanted cell attachment and, in combination with the CEPT cocktail, enabled highly efficient formation of free-floating EBs (Figures S1C and S1D). Again, enzyme-free passaging with EDTA, which obviates an offline centrifugation step, was ideal for fully automated EB production. As expected, EB formation from hESCs and hiPSCs and comparison of manual and automated cell culture by using the standardized ScoreCard method (Tsankov et al., 2015) showed multi-lineage differentiation potential (Figure S1E).

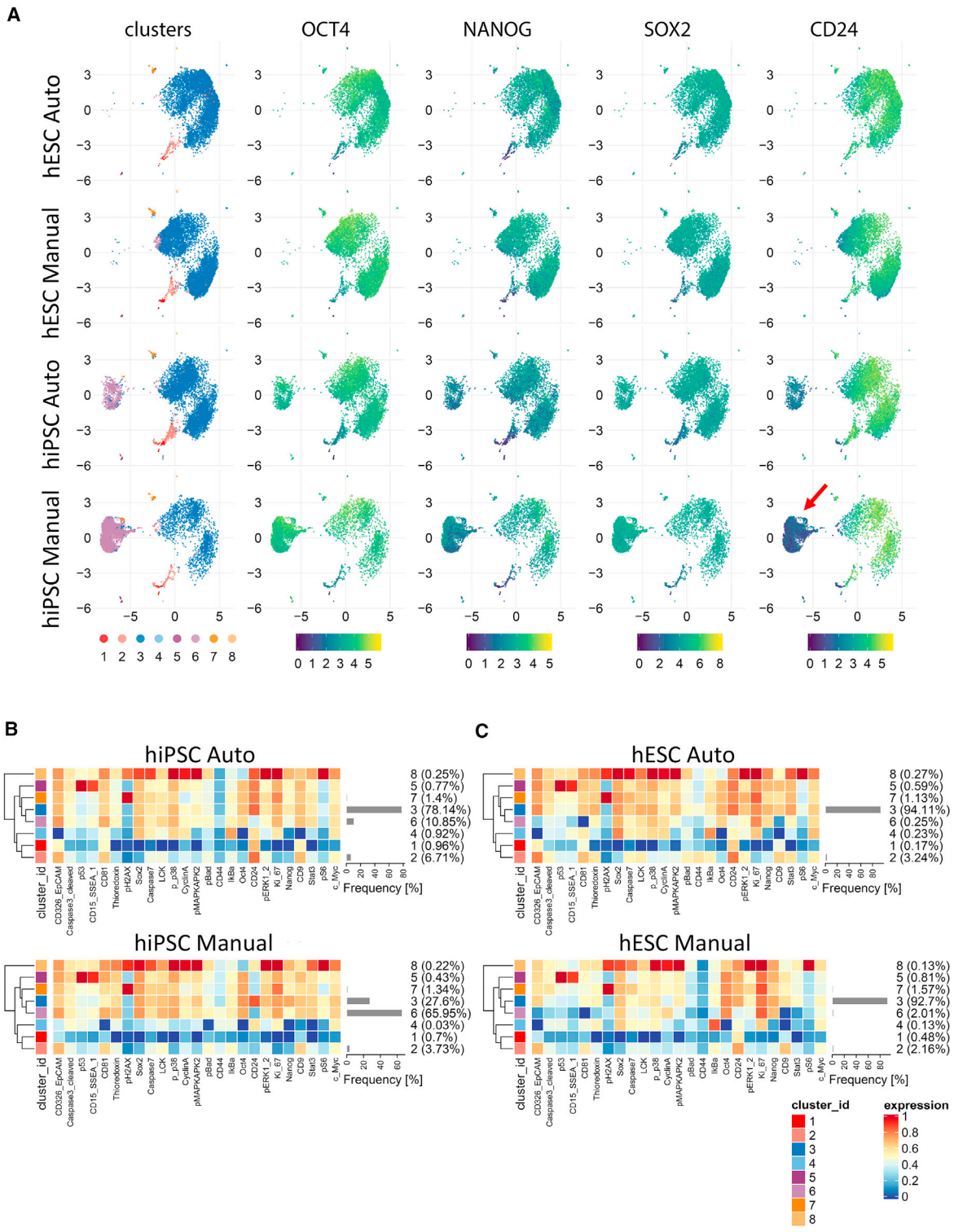

Figure 4. Mass cytometry of hiPSCs and hESCs and comparison of manual and automated cell culture

(A) Uniform manifold approximation and projection (UMAP) plots showing subpopulations of cells within each group organized into eight clusters identified by FlowSOM and ConsensusClusterPlus algorithms. Cluster 6 was prominent in hiPSCs (LiPSC-GR1.1) when cultured manually and its representation was mitigated by automated culture. Core pluripotency markers OCT4, NANOG, and SOX2 were expressed at

(legend continued on next page)

Of note, a difference in spontaneous endoderm differentiation was observed when comparing hiPSCs (LiPSC-GR1.1) to hESCs (WA09). This difference is likely due to the absence of endoderm-promoting factors in Essential 6 (E6) medium, which is known to favor differentiation into ectoderm (Lippmann et al., 2014). Indeed, in adherent cultures using a commercial kit for directed differentiation, both cell lines efficiently produced endodermal cells (Figures 5 and S3).

Controlled multi-lineage differentiation in monolayer cultures

While spontaneous EB differentiation is useful for certain applications, directed differentiation under adherent monolayer conditions is highly desirable for developing scalable protocols for different lineages. Hence, we established automated protocols for directed differentiation into the three embryonic germ layers. For neural differentiation, hPSCs were cultured in E6 medium containing the bone morphogenetic protein (BMP) pathway inhibitor LDN-193189 (100 nM) and the transforming growth factor (TGF) β pathway inhibitor A83-01 (2 μM). Simultaneous inhibition of these pathways is typically referred to as dual-SMAD inhibition (dSMADi) (Chambers et al., 2009; Singec et al., 2016). For mesodermal and endodermal differentiation, we utilized standardized kits from a commercial vendor (experimental procedures). Stock solutions of different reagents can be stored in the chilling unit of the CTST (Figure 1), and the robotic arm can add fresh reagents during daily medium changes. By using these protocols, we were able to efficiently generate cultures with ectodermal (PAX6), mesodermal (Brachyury), and endodermal (SOX17) precursors as demonstrated by western blotting and immunocytochemistry (Figures 5A, 5B, and S3A). To confirm efficient automated multi-lineage differentiation, we performed single-cell RNA-seq analysis of lineage-committed precursor cells derived from either hiPSCs (Figures 5C and 5D) or hESCs (Figures S3B and S3C). We analyzed a total of 19,759 cells for the hiPSC line and a total of 16,582 cells for the hESC line. For both independently tested cell lines, comparison of transcriptomes by unsupervised clustering revealed distinct signatures for pluripotent, ectodermal, mesodermal, and endodermal cells (Figures 5C and S3B). Similarly, a heatmap analysis for typical lineage-specific markers demonstrated distinct molecular signatures for pluripotent and differentiated germ layer cells (Figures 5D and S3C). Comparison of cultures generated either manually or robotically, showed similar quantitative polymerase chain reaction (qPCR) expression profiles for ectodermal, mesodermal, and endodermal markers (Figure S4). Interestingly, some genes, such as *NES*, *TUBB3*, *HES4*, *MAP2*, *Brachyury*, *VIM*, *NODAL*, and *ABCA4*, were expressed at higher levels when cultures were differentiated robotically versus manually (Figure S4). Last, comparing automated hiPSCs and hESCs cultures with each other revealed a high degree of similarity among pluripotent and lineage-committed progeny (Figure 5E). Together, the robotic cell differentiation protocols established here generated primary embryonic germ layers with high efficiency and reproducibility.

Scalable production of functional human neurons

The translation of hiPSCs depends on controlled and scalable differentiation into diverse cellular phenotypes that can be used for disease modeling, drug screening, and cell therapies. We asked if executing complex multi-step protocols over several weeks could be performed by using robotic cell culture in a fully automated "touch-and-go" fashion. Hence, we developed a cost-efficient differentiation protocol that utilizes the dSMADi strategy followed by culturing cells as neurospheres and then replating them for further maturation and analysis (Figures 6A–6C). Most neuronal cells (>90%) generated by using this simple protocol (Figure 6A) expressed neuronal markers β-III-tubulin (TUJ1) and microtubule-associated protein 2 (MAP2) at day 30 (Figures 6D, 6E, and S5A). Expression of transcription factors CUX1 (a marker for cortical layers 2/3) and CTIP2 (a marker for cortical layers 5/6) indicated the generation of specific forebrain neurons (Figures 6D and 6E) that were generated at higher numbers using automated versus manual differentiation (Figure S5A). Moreover, specific antibodies against vesicular glutamate transporter 1 (vGLUT1) and γ-aminobutyric acid (GABA) suggested that cultures contained a mixed population of cells, with the majority (>80%) representing glutamatergic neurons (Figures 6F, 6G, and S5A).

similar levels across clusters. Surface-antigen CD24 was expressed at a considerably higher level in cluster 6 in hiPSCs cultured manually (red arrow).

(B) Heatmaps comparing protein expression levels for each analyzed marker in individual clusters and the abundance of the clusters within the hiPSC populations (LiPSC-GR1.1) cultured manually or by automation. Manual culture led to a large proportion of CD24-negative cells, 66% versus 11% in automated culture.

(C) Heatmaps of protein expression levels and cluster abundances in hESCs (WA09) after manual and automated cell culture. The abundance of the major cluster 3 was similar in both culture conditions, and CD24-negative cluster 6 was represented at a negligible level. UMAP plots were constructed from 8,000 single cells per sample (n = 4 independent experiments) obtained from two independent cell lines (A–C). CyTOF data were analyzed using a modified CyTOF workflow (Robinson et al., 2017).

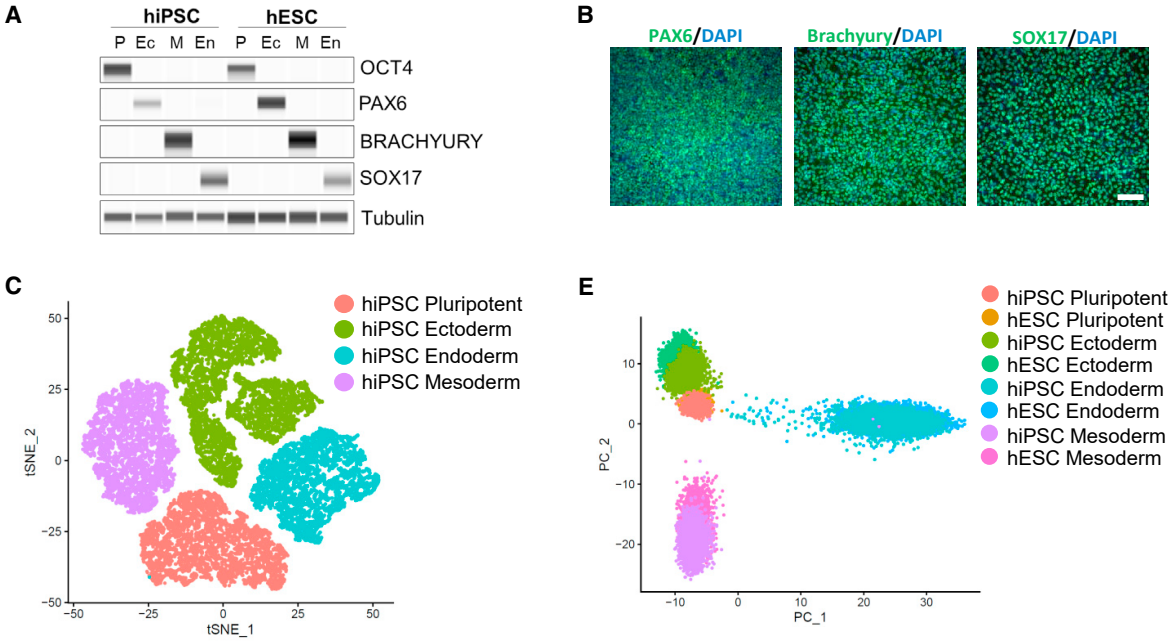

(legend on next page)

To demonstrate neuronal activity, we conducted electrophysiological analysis using the robotic Maestro APEX multi-electrode array (MEA) platform (Figure 6H). At day 30, cultures were dissociated into single cells and 140,000 neurons were seeded into a well with 16 electrodes in the presence of the CEPT cocktail (applied for 24 h to improve viability). At day 7 post-plating, an analysis of extracellular field potentials revealed spontaneous activity in hiPSC-derived neuronal cultures generated manually or robotically (Figure 6I). Similar spike shapes and amplitudes were also detected 2 weeks later in both groups (Figures 6J, S5B, and S5C). Moreover, comparing cultures generated either manually or robotically by qPCR, both cultures expressed typical neuronal markers, *SATB2*, *CUX1*, *GAD1*, *SLC6A1*, *BCL11B*, and *SLC17A7* (Figure S5D).

Standardized production of functional cardiomyocytes and hepatocytes

Derivation of large quantities of hiPSC-derived cardiomyocytes and hepatocytes is important for drug development, toxicology, and regenerative medicine (Kimbrel and Lanza, 2020; Sharma et al., 2020). To generate cardiomyocytes, we adopted a kit-based protocol for automated differentiation of hPSCs (Figure 7A). A western blot analysis of differentiated hESCs and hiPSCs demonstrated strong induction of TNNI3 (cardiac troponin) and transcription factor NKX2.5 at day 14 (Figure 7B). Immunocytochemistry and flow cytometry showed that 80% to 90% of cells expressed cardiomyocyte-specific markers TNNI3 and ACTC1 (α-cardiac actin) irrespective of manual or robotic differentiation (Figures 7C, 7D, S6A, and S6B). Moreover, a comparison of manually and robotically differentiated cultures (day 24) indicated similar expression levels of typical cardiomyocyte markers as measured by qPCR (Figure S6H). A functional analysis confirmed that cardiomyocytes were active and spontaneously beating as measured by MEA (Figures 7E and S6C). An analysis of field potentials documented spontaneous cardiomyocyte activity (Figures 7G and S6E). Beat-to-beat variance analysis showed that cardiomyocytes exhibited regular and consistent beat intervals, confirming the presence of non-arrhythmic cardiomyocytes, field potential durations, and conduction velocities that were comparable in cultures generated by manual and automated differentiation (Figures 7F, 7G, and S6D–S6G).

Next, we established an automated protocol for hepatocyte differentiation using the CTST platform. A 20-day protocol (Mallanna and Duncan, 2013) was adopted to generate human hepatocytes entirely in scaled-down 384-well plates compatible with high-throughput screening (Figure 7H). Immunocytochemical analysis at day 10 showed that >80% of cells, differentiated manually and robotically, expressed endodermal markers FOXA2 and HNF4A (Figure 7I and S7A–S7C). Comparison of cultures at day 10, generated either manually or robotically, showed similar expression levels for *FOXA2*, *GATA4*, and *GATA6* as measured by qPCR analysis (Figure S7F). By day 20, hepatocytes expressed HNF4A, α-fetoprotein (AFP), and albumin (Figures 7J, 7K, S7D, and S7E). qPCR showed that cultures differentiated manually or robotically exhibited similar levels of gene expression for *HNF4A*, *AFP*, *Albumin*, *APOA1*, *SLC10A1*, *ASGR1*, *CYP3A4*, *CYP2D6*, and *CYP3A7* (Figure S7G).

Zika virus infection of robotically generated cardiomyocytes and hepatocytes

To demonstrate the utility of robotically differentiated cells, we performed translationally relevant assays. Human cellular models provide unique opportunities to better understand Zika virus (ZIKV) pathobiology (Qian et al., 2016; Tang et al., 2016; Zhou et al., 2017). Accordingly, we found that robotically generated cardiomyocytes and hepatocytes were susceptible to ZIKV infection after viral exposure for 24 h (Figures S8A and S8B). Moreover, since intrauterine ZIKV infections can lead to microcephaly in the developing human embryo by selectively damaging neural stem cells (NSCs) (Martinot et al., 2018), in a separate study we robotically generated NSCs sufficient for 184 plates (384-well format) and performed systematic genome-wide knockdown screens to identify host factors that can protect from

Figure 5. Controlled multi-lineage differentiation of hPSCs by using CTST

(A) Western blot of hiPSCs (LiPSC-GR1.1) and hESCs (WA09) before (OCT4) and after differentiation into ectoderm (PAX6) at day 7, mesoderm (Brachyury) at day 5, and endoderm (SOX17) at day 5. Tubulin was used as loading control.

(B) Immunocytochemical analysis of hiPSC (LiPSC-GR1.1)-derived ectoderm (PAX6) at day 7, endoderm (SOX17) at day 5, and mesoderm (Brachyury) at day 5. Cultures were differentiated by CTST. Scale bar, 200 μm.

(C) Single-cell RNA-seq of pluripotent and differentiated cultures (LiPSC-GR1.1).

(D) Heatmap showing the highly expressed genes for pluripotent cells (LiPSC-GR1.1) and differentiated cultures representing ectoderm (day 7), endoderm (day 5), and mesoderm (day 5).

(E) Comparison of undifferentiated and differentiated hESCs (WA09) and hiPSCs (LiPSC-GR1.1) shows that gene expression signatures are similar. Data are from n = 4 biological replicates using two independent cell lines (A and B). Data are from n = 19,759 or 16,582 single cells obtained from n = 4 independent experiments using two independent cell lines (C–E). Cell counts for hiPSCs: 4,772 pluripotent, 6,457 ectoderm, 4,160 endoderm, and 4,370 mesoderm. Cell counts for hESCs: 3,627 pluripotent, 5,062 ectoderm, 4,267 endoderm, and 3,626 mesoderm. Single-cell RNA-seq data were analyzed in the Seurat R package.

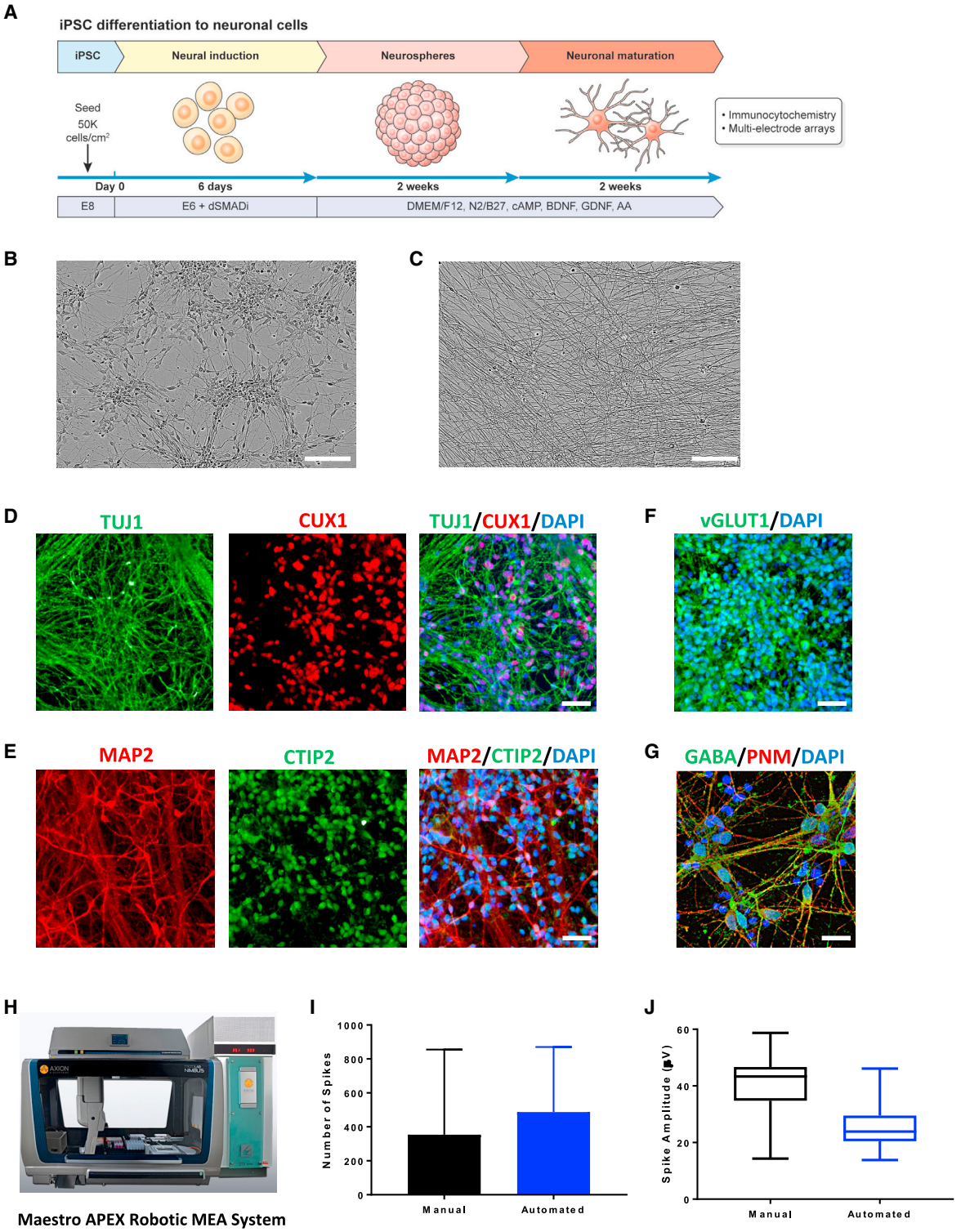

Figure 6. Robotic scalable production of hiPSC (LiPSC-GR1.1)-derived human neurons

(A) Neuronal differentiation strategy established for automated cell culture.

(B) Phase-contrast image showing a typical neuronal culture (day 30). Scale bar, 200 μm.

(C) Neurons develop a dense network of neurites upon maturation (day 50). Scale bar, 200 μm.

(D–F) hiPSC-derived cortical neurons (day 40) immunostained for (D) TUJ1 and CUX1, (E) MAP2 and CTIP2, and (F) vGLUT. Scale bar, 50 μm.

(legend continued on next page)

ZIKV infection (data not shown). Collectively, these studies showed that the automated production of different neural and non-neural cell types can be established under standardized scale-up and scale-down conditions (Table S5) enabling high-throughput genetic and chemical screens.

DISCUSSION

Cell reprogramming has allowed the generation of thousands of new hiPSC lines over the last decade. The ever-increasing number of new cell lines, including concerted efforts to generate, biobank, and distribute large numbers of cell lines derived from ethnically diverse individuals and patients with genetic diseases (Soares et al., 2014b), reinforces the need for implementing high-throughput cell culture methods that can be used as cost-efficient, standardized, and safe SOPs. It would be ideal if the production and quality testing of new hiPSC lines could be performed after employing the same reprogramming method (e.g., Sendai virus, episomal plasmids), consistently using the same chemically defined media and reagents and performing the same cell culture practices.

Currently, the culture and differentiation of hiPSC lines pose significant technical and scientific challenges for basic and translational research. Uniform and standardized processing of multiple cell lines and manufacturing various lineage-specific cell types in parallel are particularly cumbersome and inefficient for large-scale projects. Relying on a small number of cell lines for modeling human diseases and studying gene effects (e.g., population genetics) may lead to underpowered results (Cahan and Daley, 2013; Sharma et al., 2020). Another challenge is continuous passage of self-renewing hPSCs, while cell differentiation experiments are initiated in parallel. Therefore, to increase experimental reproducibility, the production of large cell quantities at a given passage number and establishing an original batch (CryoPause) was recommended (Wong et al., 2017). Automation can help to overcome these challenges, reduce the burden of manual hiPSC culture, and contribute to improving overall experimental reproducibility. Our daily experience using the CTST over the last 5 years convinced us of the advantages and versatility of automated cell culture. High-quality hPSCs can be expanded, cryopreserved, differentiated, and utilized on demand in large flasks or assay-ready microplates. In contrast with previous studies that also used the CTST system (Table S6), we were able to automate and characterize all essential steps of hiPSC culture, including massive cell expansion (Figure 2Q) and controlled multi-lineage differentiation yielding functional cell types. Systematic cell characterization experiments using complementary methods demonstrated that cells cultured manually or robotically were qualitatively similar, further supporting the notion that industrial-scale culture of hiPSCs is feasible and not limited by the availability, work schedule, and manual labor of specially trained scientists.

The combined use of E8 medium, VTN-N coating, enzyme-free cell passaging, and the CEPT cocktail was optimal for automated cell culture. Previous studies also reported improved culture of hPSCs in E8 medium compared with traditional feeder-based methods (Wang et al., 2013; Wong et al., 2017). In general, spontaneous cell differentiation and contamination with unwanted cells might be a challenge when culturing large quantities of hPSCs in a high-throughput fashion. The advantage of using CTST is that cells can be expanded as adherent cultures, while other 3D methods and suspension cultures (e.g., bioreactors, stirring tanks) will make metabolite and oxygen exchange less controlled, expose cells to shear stress, and lead to the merging of free-floating spheres (Hookway et al., 2016; Liu et al., 2014; Schwedhelm et al., 2019; Singec et al., 2006). However, spontaneous differentiation may also occur in adherent cultures after repeated enzymatic passaging (Barbaric et al., 2014; Garitaonandia et al., 2015; Wang et al., 2013), which can be avoided by using enzyme-free approaches such as EDTA. Based on our experience with growing cell lines in E8 medium over several years, spontaneous differentiation has not been a limiting factor for automated cell culture described here. Indeed, it is possible that the use of E8 medium, EDTA, and the cytoprotective CEPT cocktail may help to minimize the risk of spontaneous differentiation. Future work and data sharing across different laboratories using automated cell culture will help to further establish this notion. Last, all experiments in this study were carried out using the CTST system in a preclinical research setting (BSL-2). As other robotic cell culture systems are becoming available (e.g., Celltrio), the next critical step toward the development of clinical-grade cellular products should be the establishment and testing of automated systems that are compatible with good manufacturing practice (GMP) guidelines.

(G) hiPSC-derived neuronal cells (day 40) showing immunoreactivity for inhibitory neurotransmitter GABA. Scale bar, 20 μm.
(H) Robotic MEA platform used for high-throughput electrophysiology and functional cell characterization.
(I and J) Comparison of (I) spontaneous neuronal spikes and (J) spike amplitudes in hiPSC-derived cultures after 6 weeks of manual or robotic cell differentiation as measured by MEA. Representative data are expressed as mean ± SD, n > 3 biological replicates (B–G, I, J). $p > 0.5$, unpaired *t* test.

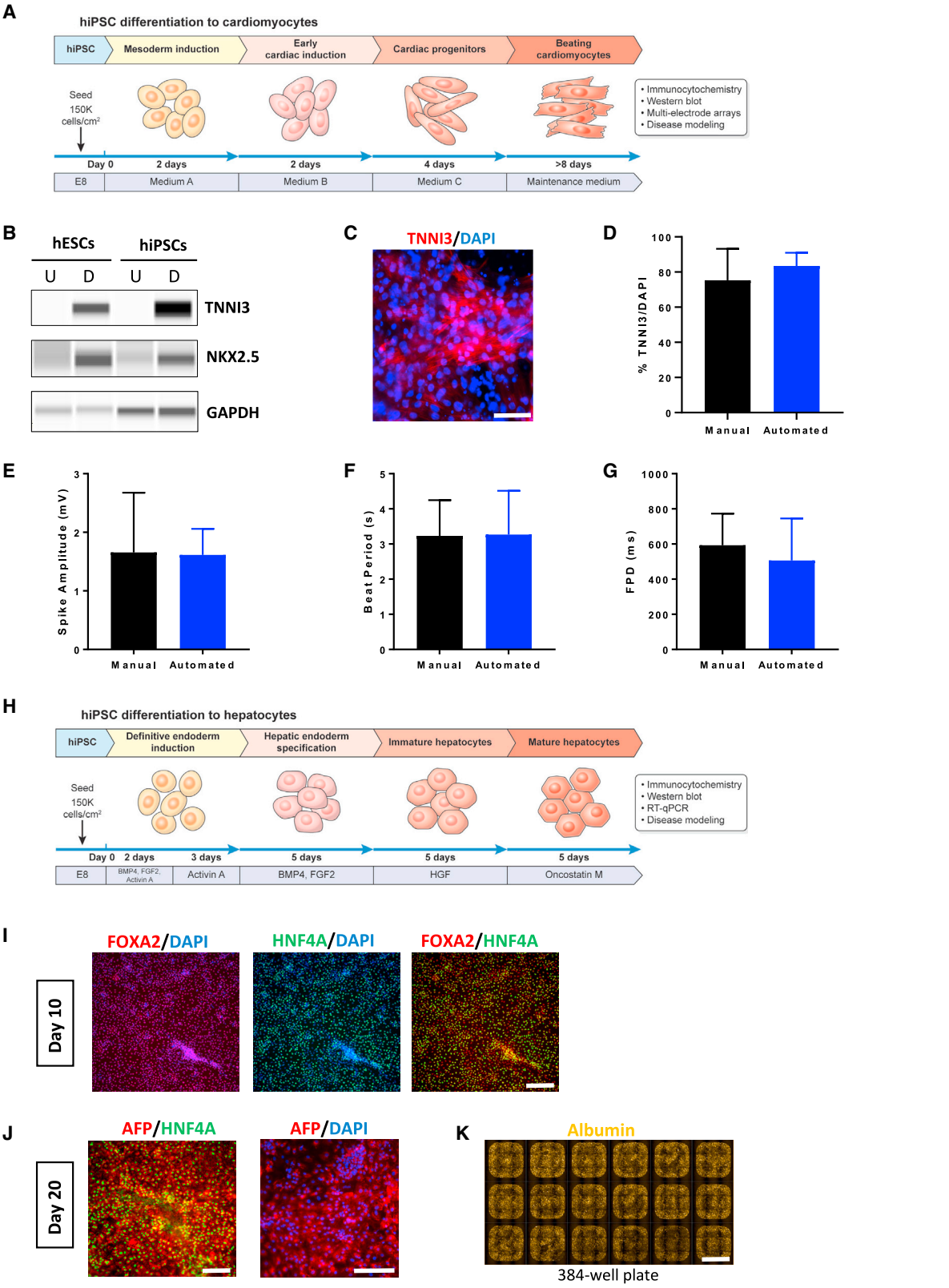

(legend on next page)

EXPERIMENTAL PROCEDURES

Detailed descriptions of experimental procedures can be found in the supplemental information.

Automated and manual cell culture

All hESC and hiPSC lines (Table S1) were maintained under feeder-free conditions in E8 medium (Thermo Fisher) and VTN-N-coated (Thermo Fisher) microplates or T175 flasks as described in the supplemental information.

Cell culture medium analysis

Medium analyses were done using a Vi-Cell MetaFLEX Bioanalyte analyzer (Beckman). Spent cell culture medium was analyzed and evaluated for pH, pO_2, pCO_2, glucose, lactate, and electrolytes every 24 h.

Live-cell metabolic assays using the Seahorse XF analyzer

The oxygen consumption rate (OCR) and extracellular acidification rate (ECAR) were analyzed using a Seahorse XF-96 analyzer (Agilent) according to the manufacturer's protocol. OCR and ECAR values were normalized to total cells per well.

MEA

Electrophysiology was performed on the Maestro APEX robotic platform (Axion Biosystems) as described in the supplemental information.

Mass CyTOF

Following single-cell dissociation, hESCs/iPSCs were stained and labeled for CyTOF analysis using the Maxpar Human ES/iPS Phenotyping Panel Kit (Fluidigm) and other lanthanide metal-labeled antibodies (Table S4).

Single-cell RNA library preparation and sequencing

hESCs, hiPSCs, and their derived cell types were single-cell dissociated, loaded on a Chromium Controller (10× Genomics) to generate single-cell gel bead-in-emulsions (GEMs) and barcoding. Libraries were sequenced on an Illumina HiSeq 3,000.

Analysis of single-cell RNA-seq

Details of the analysis procedure are described in the supplemental information.

Automated and manual differentiation into embryonic germ layers

Endoderm and mesoderm differentiations were induced using the TeSR-E8 optimized STEMdiff Definitive Endoderm Kit (STEMCELL Technologies) or STEMdiff Mesoderm Induction Medium (STEMCELL Technologies). Endoderm and mesoderm cells were analyzed on day 5. Ectoderm differentiation was induced using E6 medium supplemented with LDN-193189 (100 nM, Tocris) and A83-01 (2 μM, Tocris) and cells were analyzed on day 7. All automated and manual protocols were performed in parallel as described in the supplemental information.

Automated and manual neuronal differentiation

Neuronal differentiation is summarized (Figure 6A) and described in the supplemental information.

Automated and manual cardiomyocyte differentiation

Cardiomyocyte differentiation is summarized (Figure 7A) and described in the supplemental information.

Automated and manual hepatocyte differentiation

Hepatocyte differentiation was performed as summarized (Figure 7H) and described in the supplemental information.

Data and code availability

Raw sequencing data generated in this study can be found in the NCBI SRA database under the Bioproject accession number PRJNA657268.

Analysis code is available at https://github.com/cemalley/Tristan_methods.

SUPPLEMENTAL INFORMATION

Supplemental information can be found online at https://doi.org/10.1016/j.stemcr.2021.11.004.

Figure 7. Characterization of cardiomyocytes and hepatocytes derived by automated cell culture

(A) Overview of cardiomyocyte differentiation protocol.

(B) Western blot showing induction of cardiac troponin and NKX2.5 in undifferentiated (abbreviated as U) and differentiated (abbreviated as D) hESCs (WA09) and hiPSCs (LiPSC-GR1.1) at day 24. GAPDH was used as a loading control.

(C and D) (C) Immunocytochemistry and (D) quantification shows that hiPSC-derived cardiomyocytes express cardiac troponin (day 24). Scale bar, 75 μm.

(E) Comparison of spontaneous spike amplitudes in hiPSC-derived cardiomyocytes differentiated manually or robotically (day 24).

(F and G) Comparison of (F) beat periods and (G) field potential duration in cardiomyocyte cultures (LiPSC-GR1.1) differentiated manually or robotically and measured by MEA (day 24).

(H) Overview of hepatocyte differentiation protocol.

(I) Immunocytochemistry at day 10 shows most hiPSC (LiPSC-GR1.1)-derived cells express FOXA2 and HNF4A. Scale bar, 200 μm.

(J) hiPSCs (LiPSC-GR1.1) differentiated into hepatocytes express α-fetoprotein (AFP) and HNF4A (day 20). Scale bar, 200 μm.

(K) Immunocytochemistry showing albumin-expressing hepatocytes robotically differentiated in a 384-well plate. Representative overview of 18 whole wells containing hepatocytes. Scale bar, 2 mm. Representative data are expressed as mean ± SD, $n > 3$ biological replicates. $p > 0.5$, unpaired t test.

AUTHOR CONTRIBUTIONS

C.A.T. and I.S. conceived the study and experiments. C.A.T., P.O., J.S., P.C., V.M.J., Y.G., Y.J., C.B., E.B., S.K.M., D.D., and M.J.I. performed experiments. C.A.T., P.O., J.S., C.M, P.C., V.M.J., J.B., S.K.M., M.J.I., T.C.V., S.M., A.S., and I.S. contributed to data analysis and discussions. C.T. and I.S. wrote the manuscript.

CONFLICT OF INTERESTS

A.S. and I.S. are co-inventors on a US Department of Health and Human Services patent application covering CEPT and its use.

ACKNOWLEDGMENTS

We thank all our colleagues at NCATS, DPI. We are grateful to Alan Hoofring and Ethan Tyler from the NIH Medical Arts Design Section for their technical expertise. We also acknowledge funding from the NIH Common Fund (Regenerative Medicine Program), the NIH HEAL Initiative and, in part, the intramural research program of NCATS.

Received: August 21, 2020
Revised: November 2, 2021
Accepted: November 4, 2021
Published: December 2, 2021

REFERENCES

Aijaz, A., Li, M., Smith, D., Khong, D., Leblon, C., Fenton, O.S., Olabisi, R.M., Libutti, S., Tischfield, J., Maus, M.V., et al. (2018). Biomanufacturing for clinically advanced cell therapies. Nat. Biomed. Eng. *2*, 362–376.

Archibald, P.R.T., Chandra, A., Thomas, D., Chose, O., Massouridès, E., Laâbi, Y., and Williams, D.J. (2016). Comparability of automated human induced pluripotent stem cell culture: a pilot study. Bioproc. Biosyst. Eng. *39*, 1847–1858.

Barbaric, I., Biga, V., Gokhale, P.J., Jones, M., Stavish, D., Glen, A., Coca, D., and Andrews, P.W. (2014). Time-lapse analysis of human embryonic stem cells reveals multiple bottlenecks restricting colony formation and their relief upon culture adaptation. Stem Cell. Reports *3*, 142–155.

Cahan, P., and Daley, G.Q. (2013). Origins and implications of pluripotent stem cell variability and heterogeneity. Nat. Rev. Mol. Cell Biol. *14*, 357–368.

Chambers, S.M., Fasano, C.A., Papapetrou, E.P., Tomishima, M., Sadelain, M., and Studer, L. (2009). Highly efficient neural conversion of human ES and iPS cells by dual inhibition of SMAD signaling. Nat. Biotechnol. *27*, 275–280.

Chen, G., Gulbranson, D.R., Hou, Z., Bolin, J.M., Ruotti, V., Probasco, M.D., Smuga-Otto, K., Howden, S.E., Diol, N.R., Propson, N.E., et al. (2011). Chemically defined conditions for human iPSC derivation and culture. Nat. Methods *8*, 424–429.

Chen, Y., Tristan, C.A., Chen, L., Jovanovic, V.M., Malley, C., Chu, P.H., Ryu, S., Deng, T., Ormanoglu, P., Tao, D., et al. (2021). A Versatile Polypharmacology Platform Promotes Cytoprotection and Viability of Human Pluripotent and Differentiated Cells (Springer US).

Daniszewski, M., Crombie, D.E., Henderson, R., Liang, H.H., Wong, R.C.B., Hewitt, A.W., and Pébay, A. (2018). Automated cell culture systems and their applications to human pluripotent stem cell studies. SLAS Technol. *23*, 315–325.

Garitaonandia, I., Amir, H., Boscolo, F.S., Wambua, G.K., Schultheisz, H.L., Sabatini, K., Morey, R., Waltz, S., Wang, Y.C., Tran, H., et al. (2015). Increased risk of genetic and epigenetic instability in human embryonic stem cells associated with specific culture conditions. PLoS One *10*, 1–25.

Gu, W., Gaeta, X., Sahakyan, A., Chan, A.B., Hong, C.S., Kim, R., Braas, D., Plath, K., Lowry, W.E., and Christofk, H.R. (2016). Glycolytic metabolism plays a functional role in regulating human pluripotent stem cell state. Cell Stem Cell *19*, 476–490.

Guo, H., Tian, L., Zhang, J.Z., Kitani, T., Paik, D.T., Lee, W.H., and Wu, J.C. (2019). Single-cell RNA sequencing of human embryonic stem cell differentiation delineates adverse effects of nicotine on embryonic development. Stem Cell. Reports *12*, 772–786.

Hookway, T.A., Butts, J.C., Lee, E., Tang, H., and McDevitt, T.C. (2016). Aggregate formation and suspension culture of human pluripotent stem cells and differentiated progeny. Methods *101*, 11–20.

Horiguchi, I., Urabe, Y., Kimura, K., and Sakai, Y. (2018). Effects of glucose, lactate and basic FGF as limiting factors on the expansion of human induced pluripotent stem cells. J. Biosci. Bioeng. *125*, 111–115.

Jacobs, K., Zambelli, F., Mertzanidou, A., Smolders, I., Geens, M., Nguyen, H.T., Barbé, L., Sermon, K., and Spits, C. (2016). Higher-density culture in human embryonic stem cells results in DNA damage and genome instability. Stem Cell Reports *6*, 330–341.

Kimbrel, E.A., and Lanza, R. (2020). Next-generation stem cells — ushering in a new era of cell-based therapies. Nat. Rev. Drug Discov. *19*, 463–479.

Konagaya, S., Ando, T., Yamauchi, T., Suemori, H., and Iwata, H. (2015). Long-term maintenance of human induced pluripotent stem cells by automated cell culture system. Sci. Rep. *5*, 1–9.

Kuo, H.H., Gao, X., DeKeyser, J.M., Fetterman, K.A., Pinheiro, E.A., Weddle, C.J., Fonoudi, H., Orman, M.V., Romero-Tejeda, M., Jouni, M., et al. (2020). Negligible-cost and weekend-free chemically defined human iPSC culture. Stem Cell. Reports *14*, 256–270.

Lancaster, M.A., Renner, M., Martin, C.A., Wenzel, D., Bicknell, L.S., Hurles, M.E., Homfray, T., Penninger, J.M., Jackson, A.P., and Knoblich, J.A. (2013). Cerebral organoids model human brain development and microcephaly. Nature *501*, 373–379.

Lippmann, E.S., Estevez-Silva, M.C., and Ashton, R.S. (2014). Defined human pluripotent stem cell culture enables highly efficient neuroepithelium derivation without small molecule inhibitors. Stem Cells *32*, 1032–1042.

Liu, N., Zang, R., Yang, S.T., and Li, Y. (2014). Stem cell engineering in bioreactors for large-scale bioprocessing. Eng. Life Sci. *14*, 4–15.

Ludwig, T.E., Levenstein, M.E., Jones, J.M., Berggren, W.T., Mitchen, E.R., Frane, J.L., Crandall, L.J., Daigh, C.A., Conard, K.R., Piekarczyk, M.S., et al. (2006). Derivation of human embryonic stem cells in defined conditions. Nat. Biotechnol. *24*, 185–187.

Mallanna, S.K., and Duncan, S.A. (2013). Differentiation of hepatocytes from pluripotent stem cells. Curr. Protoc. Stem Cell Biol. *1*, 1G.4.1–1G.4.13.

Martinot, A.J., Abbink, P., Afacan, O., Prohl, A.K., Bronson, R., Hecht, J.L., Borducchi, E.N., Larocca, R.A., Peterson, R.L., Rinaldi, W., et al. (2018). Fetal neuropathology in zika virus-infected pregnant female rhesus monkeys. Cell *173*, 1111–1122.e10.

McLaren, D., Gorba, T., Marguerie De Rotrou, A., Pillai, G., Chappell, C., Stacey, A., Lingard, S., Falk, A., Smith, A., Koch, P., et al. (2013). Automated large-scale culture and medium-throughput chemical screen for modulators of proliferation and viability of human induced pluripotent stem cell-derived neuroepithelial-like stem cells. J. Biomol. Screen. *18*, 258–268.

Niepel, M., Hafner, M., Mills, C.E., Subramanian, K., Williams, E.H., Chung, M., Gaudio, B., Barrette, A.M., Stern, A.D., Hu, B., et al. (2019). A multi-center study on the reproducibility of drug-response assays in mammalian cell lines. Cell Syst. *9*, 35–48.e5.

Osafune, K., Caron, L., Borowiak, M., Martinez, R.J., Fitz-Gerald, C.S., Sato, Y., Cowan, C.A., Chien, K.R., and Melton, D.A. (2008). Marked differences in differentiation propensity among human embryonic stem cell lines. Nat. Biotechnol. *26*, 313–315.

Panopoulos, A.D., D'Antonio, M., Benaglio, P., Williams, R., Hashem, S.I., Schuldt, B.M., DeBoever, C., Arias, A.D., Garcia, M., Nelson, B.C., et al. (2017). iPSCORE: a resource of 222 iPSC lines enabling functional characterization of genetic variation across a variety of cell types. Stem Cell. Reports *8*, 1086–1100.

Paull, D., Sevilla, A., Zhou, H., Hahn, A.K., Kim, H., Napolitano, C., Tsankov, A., Shang, L., Krumholz, K., Jagadeesan, P., et al. (2015). Automated, high-throughput derivation, characterization and differentiation of induced pluripotent stem cells. Nat. Methods *12*, 885–892.

Qian, X., Nguyen, H.N., Song, M.M., Hadiono, C., Ogden, S.C., Hammack, C., Yao, B., Hamersky, G.R., Jacob, F., Zhong, C., et al. (2016). Brain-region-specific organoids using mini-bioreactors for modeling ZIKV exposure. Cell *165*, 1238–1254.

Qin, X., Sufi, J., Vlckova, P., Kyriakidou, P., Acton, S.E., Li, V.S.W., Nitz, M., and Tape, C.J. (2020). Cell-type-specific signaling networks in heterocellular organoids. Nat. Methods *17*, 335–342.

Quadrato, G., Nguyen, T., Macosko, E.Z., Sherwood, J.L., Yang, S.M., Berger, D.R., Maria, N., Scholvin, J., Goldman, M., Kinney, J.P., et al. (2017). Cell diversity and network dynamics in photosensitive human brain organoids. Nature *545*, 48–53.

Rigamonti, A., Repetti, G.G., Sun, C., Price, F.D., Reny, D.C., Rapino, F., Weisinger, K., Benkler, C., Peterson, Q.P., Davidow, L.S., et al. (2016). Large-scale production of mature neurons from human pluripotent stem cells in a three-dimensional suspension culture system. Stem Cell Reports *6*, 993–1008.

Robinson, M.D., Nowicka, M., Krieg, C., Weber, L.M., Hartmann, F.J., Guglietta, S., Becher, B., and Levesque, M.P. (2017). CyTOF workflow: differential discovery in high-throughput high-dimensional cytometry datasets. F1000Research *6*, 1–53.

Rodin, S., Antonsson, L., Niaudet, C., Simonson, O.E., Salmela, E., Hansson, E.M., Domogatskaya, A., Xiao, Z., Damdimopoulou, P., Sheikhi, M., et al. (2014). Clonal culturing of human embryonic stem cells on laminin-521/E-cadherin matrix in defined and xeno-free environment. Nat. Commun. *5*, 1–13.

Sato, Y., Bando, H., Di Piazza, M., Gowing, G., Herberts, C., Jackman, S., Leoni, G., Libertini, S., MacLachlan, T., McBlane, J.W., et al. (2019). Tumorigenicity assessment of cell therapy products: the need for global consensus and points to consider. Cytotherapy *21*, 1095–1111.

Schwedhelm, I., Zdzieblo, D., Appelt-Menzel, A., Berger, C., Schmitz, T., Schuldt, B., Franke, A., Müller, F.J., Pless, O., Schwarz, T., et al. (2019). Automated real-time monitoring of human pluripotent stem cell aggregation in stirred tank reactors. Sci. Rep. *9*, 1–12.

Shakiba, N., White, C.A., Lipsitz, Y.Y., Yachie-Kinoshita, A., Tonge, P.D., Hussein, S.M.I., Puri, M.C., Elbaz, J., Morrissey-Scoot, J., Li, M., et al. (2015). CD24 tracks divergent pluripotent states in mouse and human cells. Nat. Commun. *6*, 1–11.

Sharma, A., Sances, S., Workman, M.J., and Svendsen, C.N. (2020). Multi-lineage human iPSC-derived platforms for disease modeling and drug discovery. Cell Stem Cell *26*, 309–329.

Singec, I., Knoth, R., Meyer, R.P., Maciaczyk, J., Volk, B., Nikkhah, G., Frotscher, M., and Snyder, E.Y. (2006). Defining the actual sensitivity and specificity of the neurosphere assay in stem cell biology. Nat. Methods *3*, 801–806.

Singec, I., Crain, A.M., Hou, J., Tobe, B.T.D., Talantova, M., Winquist, A.A., Doctor, K.S., Choy, J., Huang, X., La Monaca, E., et al. (2016). Quantitative analysis of human pluripotency and neural specification by in-depth (phospho)proteomic profiling. Stem Cell. Reports *7*, 527–542.

Soares, F.A.C., Chandra, A., Thomas, R.J., Pedersen, R.A., Vallier, L., and Williams, D.J. (2014a). Investigating the feasibility of scale up and automation of human induced pluripotent stem cells cultured in aggregates in feeder free conditions. J. Biotechnol. *173*, 53–58.

Soares, F.A.C., Sheldon, M., Rao, M., Mummery, C., and Vallier, L. (2014b). International coordination of large-scale human induced pluripotent stem cell initiatives: Wellcome Trust and ISSCR workshops white paper. Stem Cell. Reports *3*, 931–939.

Tang, H., Hammack, C., Ogden, S.C., Wen, Z., Qian, X., Li, Y., Yao, B., Shin, J., Zhang, F., Lee, E.M., et al. (2016). Zika virus infects human cortical neural progenitors and attenuates their growth. Cell Stem Cell *18*, 587–590.

Thomas, R.J., Anderson, D., Chandra, A., Smith, N.M., Young, L.E., Williams, D., and Denning, C. (2009). Automated, scalable culture of human embryonic stem cells in feeder-free conditions. Biotechnol. Bioeng. *102*, 1636–1644.

Thomson, J.A., Itskovitz-Eldor, J., Shapiro, S.S., Waknitz, M.A., Swiergiel, J.J., Marshall, V.S., and Jones, J.M. (1998). Embryonic stem cell lines derived from human blastocysts. Science *282*, 1145–1147.

Tsankov, A.M., Akopian, V., Pop, R., Chetty, S., Gifford, C.A., Daheron, L., Tsankova, N.M., and Meissner, A. (2015). A qPCR ScoreCard quantifies the differentiation potential of human pluripotent stem cells. Nat. Biotechnol. *33*, 1182–1192.

Veres, A., Faust, A.L., Bushnell, H.L., Engquist, E.N., Kenty, J.H.R., Harb, G., Poh, Y.C., Sintov, E., Gürtler, M., Pagliuca, F.W., et al.

(2019). Charting cellular identity during human in vitro β-cell differentiation. Nature *569*, 368–373.

Wang, Y., Chou, B.K., Dowey, S., He, C., Gerecht, S., and Cheng, L. (2013). Scalable expansion of human induced pluripotent stem cells in the defined xeno-free E8 medium under adherent and suspension culture conditions. Stem Cell Res. *11*, 1103–1116.

Watanabe, K., Ueno, M., Kamiya, D., Nishiyama, A., Matsumura, M., Wataya, T., Takahashi, J.B., Nishikawa, S., Nishikawa, S.I., Muguruma, K., et al. (2007). A ROCK inhibitor permits survival of dissociated human embryonic stem cells. Nat. Biotechnol. *25*, 681–686.

Wong, K.G., Ryan, S.D., Ramnarine, K., Rosen, S.A., Mann, S.E., Kulick, A., De Stanchina, E., Müller, F.J., Kacmarczyk, T.J., Zhang, C., et al. (2017). CryoPause: a new method to immediately initiate experiments after cryopreservation of pluripotent stem cells. Stem Cell. Reports *9*, 355–365.

Zhang, H., Badur, M.G., Divakaruni, A.S., Parker, S.J., Jäger, C., Hiller, K., Murphy, A.N., and Metallo, C.M. (2016). Distinct metabolic states can support self-renewal and lipogenesis in human pluripotent stem cells under different culture conditions. Cell Rep. *16*, 1536–1547.

Zhou, T., Tan, L., Cederquist, G.Y., Fan, Y., Hartley, B.J., Mukherjee, S., Tomishima, M., Brennand, K.J., Zhang, Q., Schwartz, R.E., et al. (2017). High-content screening in hPSC-neural progenitors identifies drug candidates that inhibit zika virus infection in fetal-like organoids and adult brain. Cell Stem Cell *21*, 274–283.e5.

Zunder, E.R., Lujan, E., Goltsev, Y., Wernig, M., and Nolan, G.P. (2015). A continuous molecular roadmap to iPSC reprogramming through progression analysis of single-cell mass cytometry. Cell Stem Cell *16*, 323–337.

Stem Cell Reports, Volume *16*

Supplemental Information

Robotic high-throughput biomanufacturing and functional differentiation of human pluripotent stem cells

Carlos A. Tristan, Pinar Ormanoglu, Jaroslav Slamecka, Claire Malley, Pei-Hsuan Chu, Vukasin M. Jovanovic, Yeliz Gedik, Yogita Jethmalani, Charles Bonney, Elena Barnaeva, John Braisted, Sunil K. Mallanna, Dorjbal Dorjsuren, Michael J. Iannotti, Ty C. Voss, Sam Michael, Anton Simeonov, and Ilyas Singeç

Figure S1

A

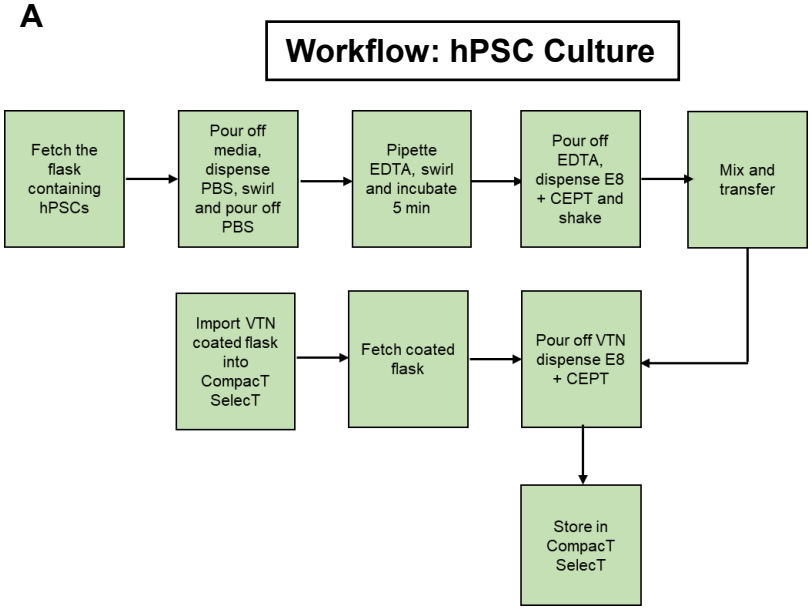

B

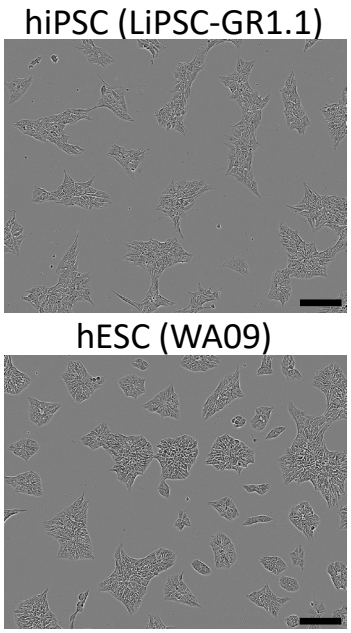

C

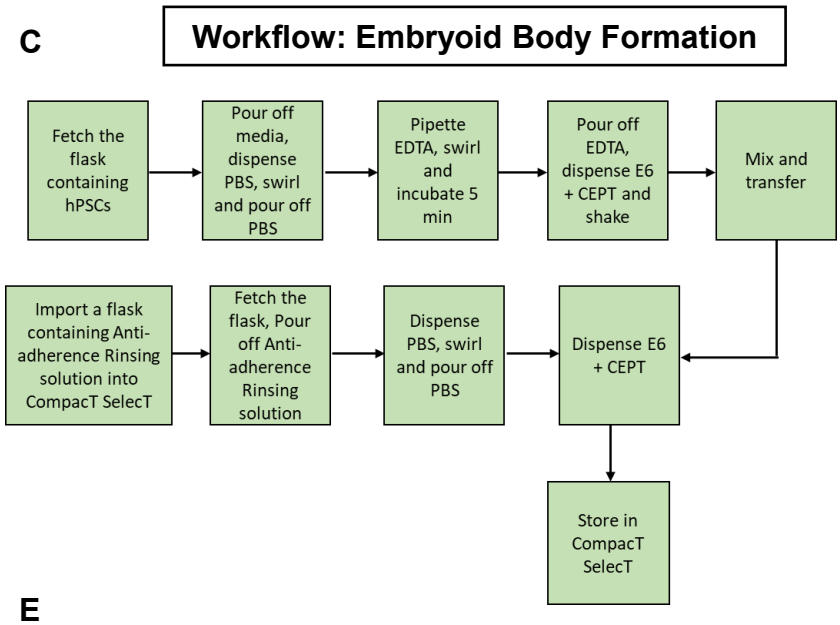

D

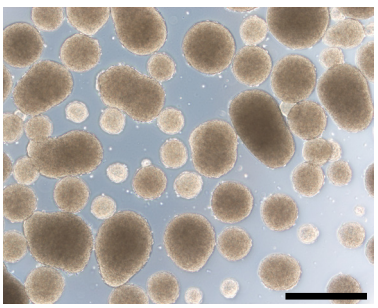

E

Sample Name	Self-renewal	Ectoderm	Mesoderm	Endoderm
hESC EB Manual	-5.05	1.30	3.07	0.56
hESC EB Automated	-4.74	1.24	2.58	0.16
hiPSC EB Manual	-0.80	0.29	0.13	-0.69
hiPSC EB Automated	0.18	0.63	0.23	-0.51

Gene expression relative to the reference standard

Upregulated						Downregulated
x > 1.5	1.0 < x ≤ 1.5	0.5 < x ≤ 1.0	-0.5 ≤ x ≤ 0.5	-1.0 ≤ x < -0.5	-1.5 ≤ x < -1.0	x < -1.5

Figure S1: Robotic workflow for culturing hPSCs and embryoid body (EB) formation
(A) Standardized protocol developed for routine culture of hPSCs using CTST under chemically defined conditions.
(B) Phase-contrast images of robotically cultured hESCs (WA09) and hPSCs (LiPSC-GR1.1) after passaging with the CEPT cocktail. Note the high quality of cultures and absence of cellular debris at 24 h post-passage.
(C) Protocol established for scalable production of EBs by using the CTST system under chemically defined conditions.
(D) Representative phase-contrast image of robotically generated EBs (day 7), which can be cultured and scaled up in large T175 flasks. Scale bar, 500 µm.
(E) ScoreCard analysis of EBs generated manually or robotically from hESCs (WA09) and hiPSCs (LiPSC-GR1.1) show differentiation potential into the three germ layers at day 7.
Data are from n > 3 biological replicates using two independent cell lines (B-C).
Representative images shown for two different cell lines. Optimal cell viability and culture was also observed using other cell lines as summarized in Table S1. Scale bar, 200 µm.

Figure S2

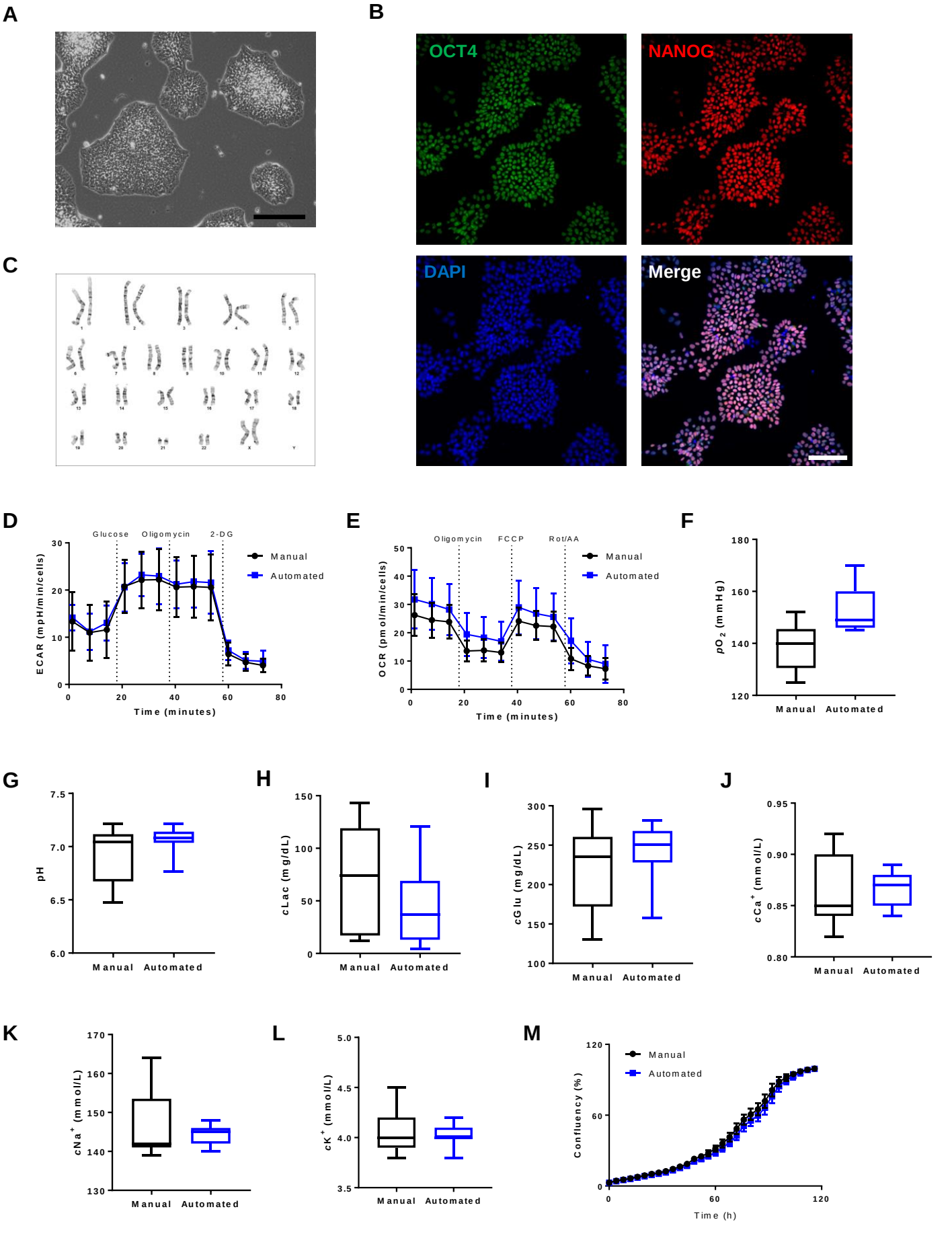
A
B
OCT4
NANOG
DAPI
Merge
C
D
Glucose
Oligomycin
2-DG
Manual
Automated
ECAR (mpH/min/cells)
Time (minutes)
E
Oligomycin
FCCP
Rot/AA
Manual
Automated
OCR (pmol/min/cells)
Time (minutes)
F
pO2 (mmHg)
Manual
Automated
G
pH
Manual
Automated
H
cLac (mg/dL)
Manual
Automated
I
cGlu (mg/dL)
Manual
Automated
J
cCa+ (mmol/L)
Manual
Automated
K
cNa+ (mmol/L)
Manual
Automated
L
cK+ (mmol/L)
Manual
Automated
M
Manual
Automated
Confluency (%)
Time (h)

Figure S2: Characterization of hESCs (WA09) cultured by CTST

(A) Representative overview of pluripotent stem cell colonies. Scale bar, 200 µm.

(B) Immunocytochemical analysis showing expression of pluripotency-associated markers OCT4 and NANOG in hESCs. Scale bar, 100 µm.

(C) Robotically cultured hESCs maintain a normal karyotype (passage 43).

(D-J) Supernatants of cultures maintained either manually or by automation were analyzed daily by using the Vi-Cell MetaFLEX Bioanalyte Analyzer (Beckman). Box plots show the variation of spent media from hESC cultures.

(K) Seahorse XF Glycolysis Stress Test profile comparison of glycolytic function in hESCs maintained by automated or manual cell culture. Cells were treated with serial injections of metabolic modulators (glucose, oligomycin, 2-deoxyglucose (2-DG)).

(L) Seahorse XF Mitochondrial Stress Test profile comparison of mitochondrial function in hESCs maintained by automated or manual cell culture. Cells were treated with serial injections of metabolic modulators (oligomycin, FCCP and Rotenone/Antimycin A (Ret/AA)).

(M) Image-based analysis comparing cell growth in hESC cultures expanded manually and robotically.

Data are expressed as mean ± SD, n > 3 biological replicates using two independent cell lines (D-M). $P > 0.5$, unpaired *t*-test.

Figure S3

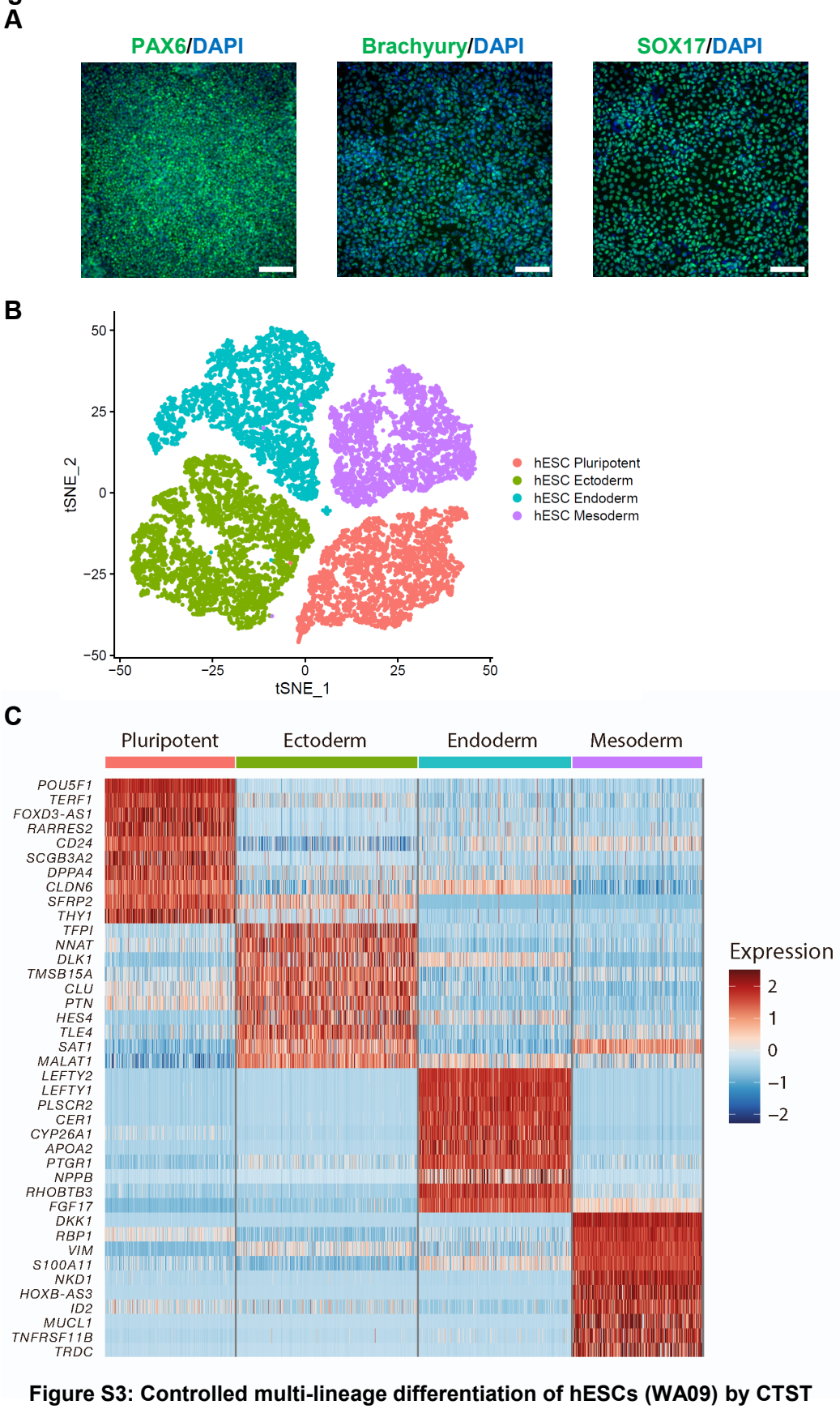

Figure S3: Controlled multi-lineage differentiation of hESCs (WA09) by CTST

(A) Immunocytochemical analysis of hESC-derived ectoderm (PAX6) at day 7, endoderm (SOX17) at day 5 and mesoderm (Brachyury) at day 5 cultures differentiated by CTST. Scale bar, 200 µm.

(B) Single-cell RNA-seq analysis of pluripotent and differentiated hESCs.

(C) Heatmap showing the highly expressed genes for pluripotent cells (WA09) and differentiated cultures representing ectoderm (day 7), endoderm (day 5) and mesoderm (day 5).

Data are from n = 4 biological replicates (A). Data are from n = 19,759 or 16,582 single cells obtained from n = 4 independent experiments using two independent cell lines (B). Single-cell RNA-seq data were analyzed in the Seurat R package. See also legend of Figure 5 for cell counts analyzed per sample.

Figure S4

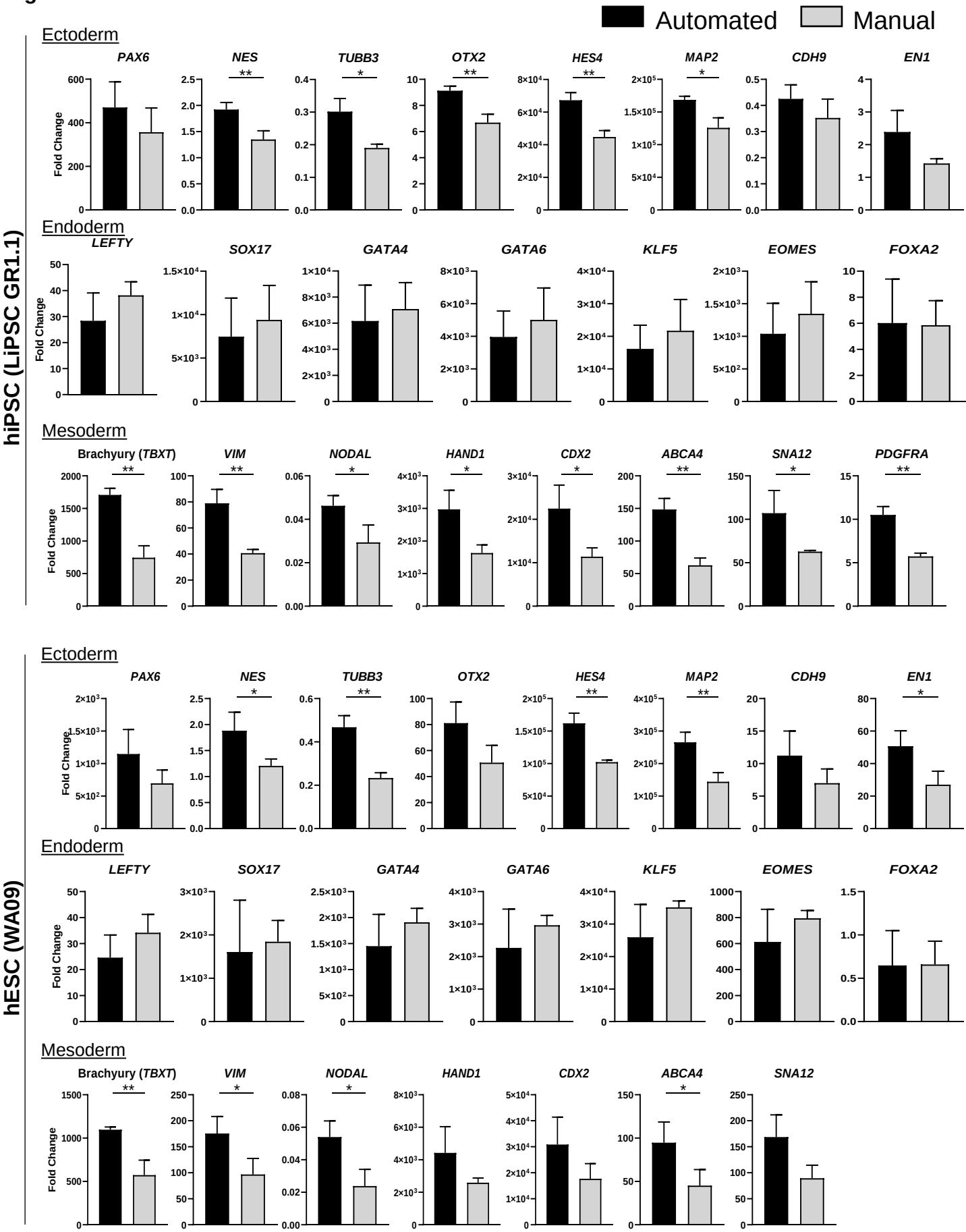

Figure S4: RT-PCR analysis and comparison of multilineage cells differentiated manually and robotically
Expression of typical gene expression of ectoderm at day 7, endoderm and mesoderm at day 5 post differentiation. Data are expressed as mean ± SD, n ≥ 3 biological replicates using hiPSCs (LiPSC-GR1.1) or hESCs (WA09). Note that *NES*, *TUBB3*, *HES4, MAP2,* Brachyury (*TBXT*), *VIM*, *NODAL* and *ABCA4* are expressed at significantly higher levels in automated versus manual differentiation. $P < 0.05$ (*) and $P < 0.01$ (**), unpaired *t*-test.

Figure S5

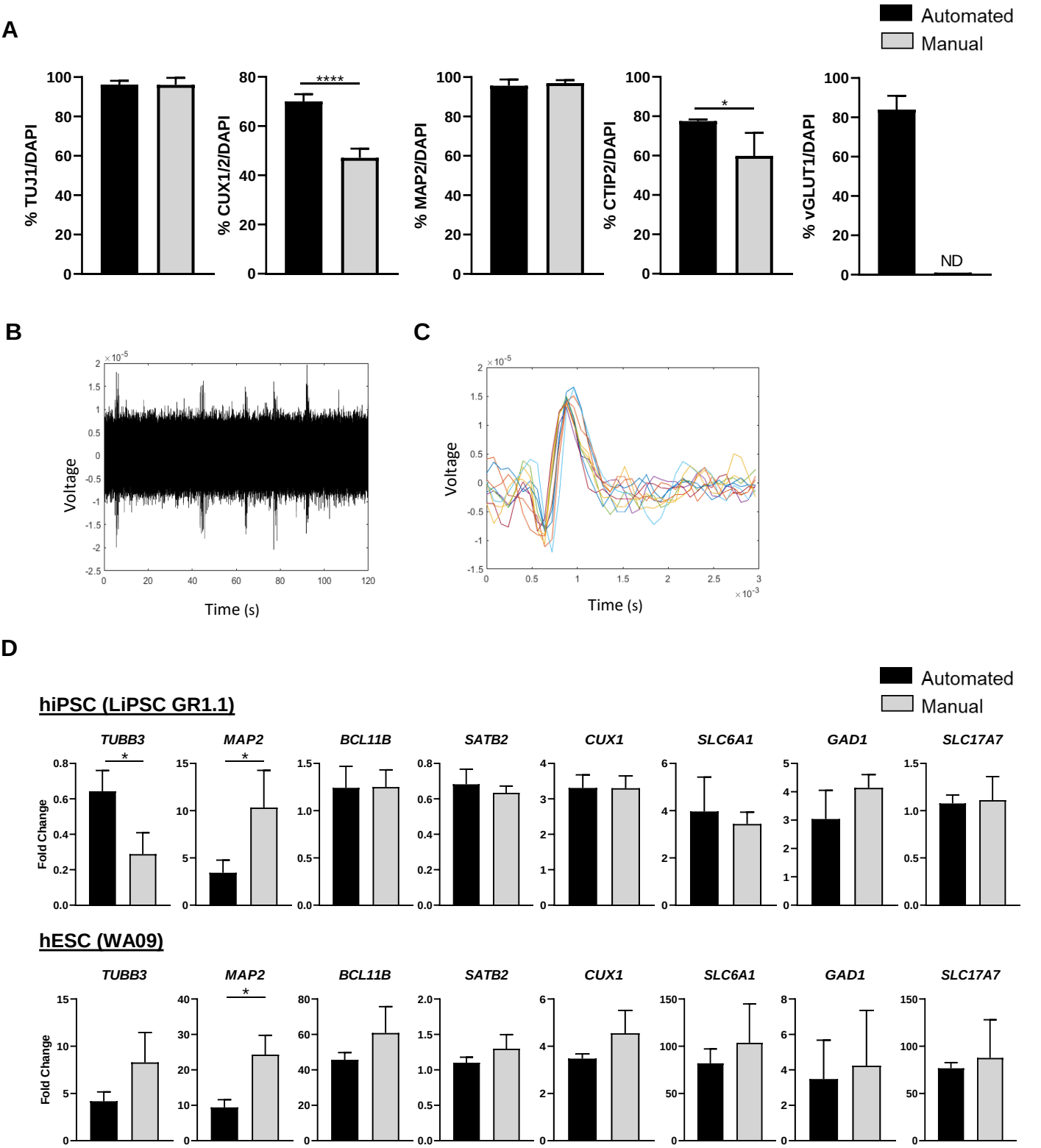

Figure S5: Quantification and characterization of neuronal cultures differentiated manually and robotically

(A) Quantification of cells expressing TUJ1, CUX1, MAP2, CTIP2, GABA and vGLUT1. Cells were differentiated for 40 days (LiPSC-GR1.1) either manually or by CTST. See also Figure 6 for representative immunostain.

(B) MEA experiment showing spontaneous neuronal activity (spike profile) at 6 weeks of robotic differentiation of hiPSCs (LiPSC-GR1.1).

(C) Representative overlay of 10 spikes detected from one channel of a MEA recording to demonstrate similarity between the spikes detected.

(D) RT-PCR analysis of typical neuronal gene expression after 6 weeks of differentiation.

Data are expressed as mean ± SD, n ≥ 3 independent fields of view (A), MEA recordings (B-C) or RT-PCR (D). $P < 0.05$ (*) and $P < 0.0001$ (****), unpaired *t*-test. N.D. indicates data not collected.

Figure S6

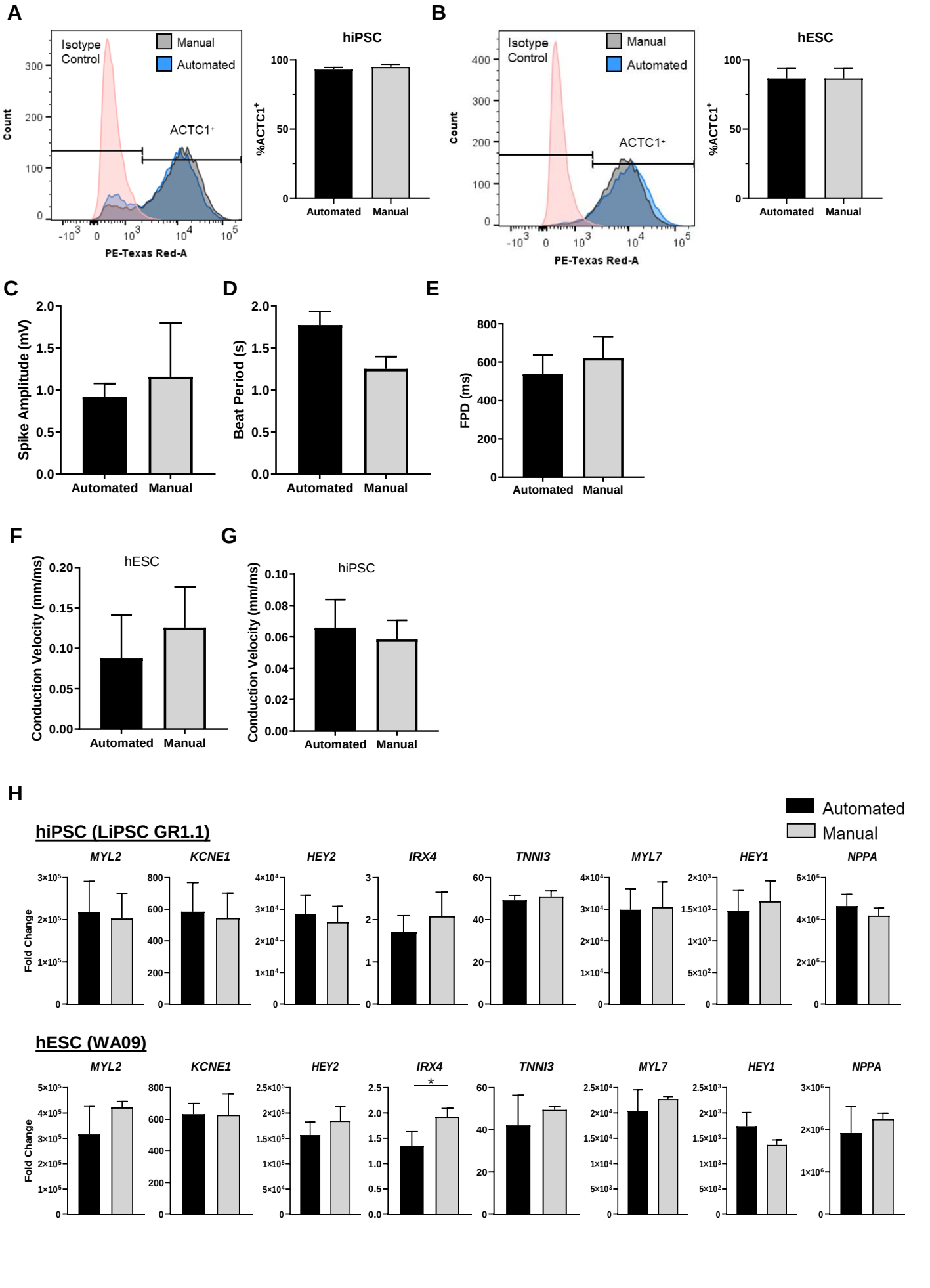
A
Isotype Control
Manual
Automated
ACTC1+
Count
PE-Texas Red-A
hiPSC
%ACTC1+
Automated
Manual
B
hESC
C
Spike Amplitude (mV)
D
Beat Period (s)
E
FPD (ms)
F
hESC
Conduction Velocity (mm/ms)
G
hiPSC
H
Automated
Manual
hiPSC (LiPSC GR1.1)
hESC (WA09)
MYL2
KCNE1
HEY2
IRX4
TNNI3
MYL7
HEY1
NPPA
Fold Change
*

Figure S6: Functional analysis and characterization of cardiomyocytes generated manually and robotically

(A, B) Flow cytometry analysis and quantification of alpha-cardiac actin (ACTC1)-expressing cells at day 24 derived from hiPSCs (LiPSC-GR1.1) and hESCs (WA09).

(C) Comparison of spontaneous spike amplitudes in cardiomyocyte cultures differentiated manually and robotically from hESCs (WA09). MEA experiment was performed at day 24.

(D) Comparison of beat periods in hESC-derived cardiomyocyte cultures (WA09) generated by manual versus automated cell differentiation. MEA experiment was performed at day 24.

(E) Comparison of field potential duration in cardiomyocyte cultures after manual and automated differentiation of hESCs (WA09) as measured by MEA on day 24.

(F, G) MEA analysis of conduction velocity in cardiomyocyte cultures derived from hESCs (WA09) and hiPSCs (LiPSC-GR1.1) after manual and robotic cell differentiation (day 24).

(H) RT-PCR analysis and comparison of typical cardiomyocyte-specific genes expressed after 24 days of manual or robotic differentiation. Note that virtually all genes tested are expressed at similar levels irrespective of manual or automated differentiation.

Data are expressed as mean ± SD, n ≥ 3 biological replicates using two independent cell lines. $P < 0.05$, unpaired *t*-test.

Figure S7

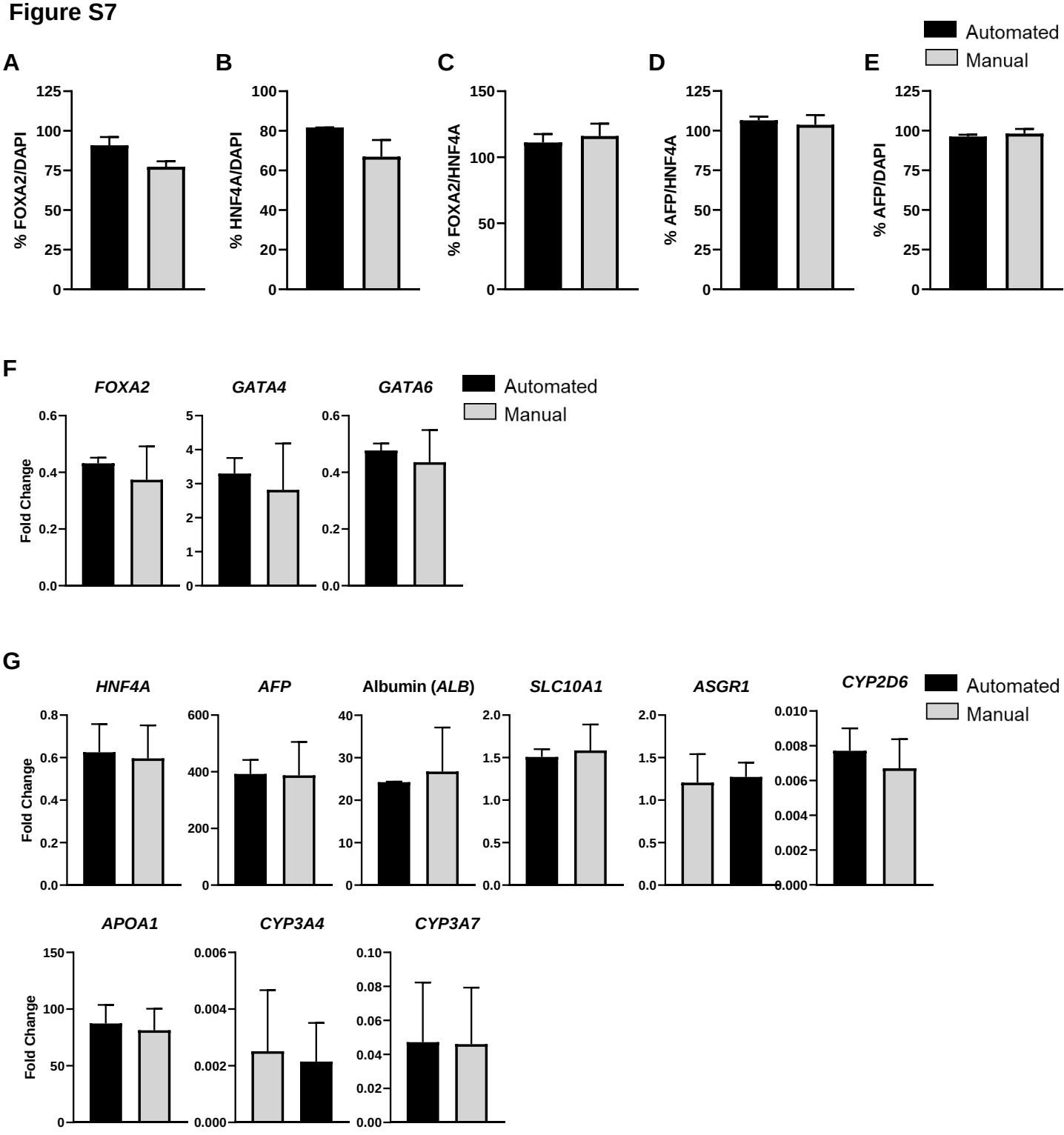

Figure S7: Quantification of endodermal and hepatic markers after manually and robotic cell differentiation

(A-E) Quantification and comparison of immunolabeled cells expressing FOXA2, HNF4A and AFP in hiPSCs cultures (LiPSC-GR1.1) differentiated into hepatocytes manually and robotically. See also Figures 7I-J for representative immunostain. Data are expressed as mean ± SD, n≥ 3 independent fields of view. $P > 0.5$, unpaired *t*-test.

(F-G) RT-PCR analysis and comparison of manual and robotic hepatocyte differentiation at day 10 and 20, respectively. Note that virtually all genes tested are expressed at similar levels irrespective of manual or automated differentiation.

Data are expressed as mean ± SD, n ≥ 3 biological replicates using the LiPSC-GR1.1 cell line. $P > 0.5$, unpaired *t*-test.

Figure S8

A

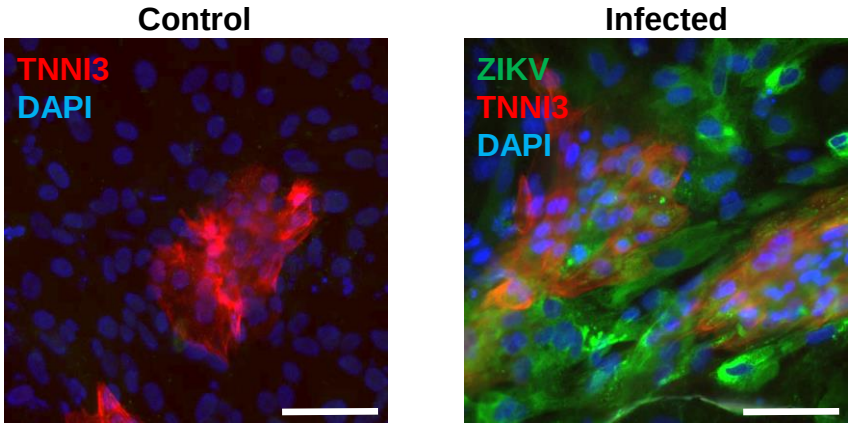

B

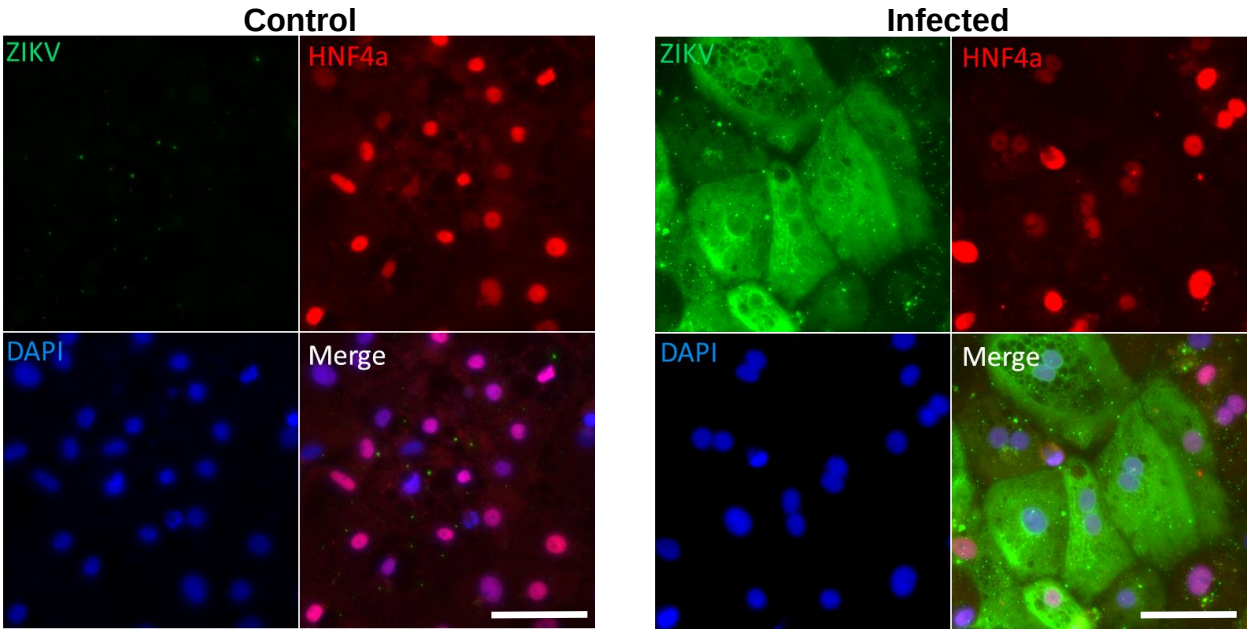

Figure S8: Infection of robotically generated cardiomyocytes and hepatocytes by ZIKV
(A) Cardiomyocytes were derived from hiPSCs (LiPSC-GR1.1) and exposed to ZIKV for 24 h. A specific antibody against flavivirus antigen shows that cells expressing cardiac troponin (TNNI3) can be infected by ZIKV. Scale bar, 75 µm.
(B) Hepatocytes were derived from hiPSCs (LiPSC-GR1.1) and exposed to ZIKV for 24 h. A specific antibody against flavivirus antigen shows that cells expressing HNF4A can be infected by ZIKV. Scale bar, 75 µm. Data are from n ≥ 3 biological replicates.

Cell Line	Source
BU NKX2.1-GFP	Boston University
CDI IPS 8621	Cellular Dynamics
GM23225	Coriell
GM23279	Coriell
GM23476	Coriell
GM23720	Coriell
GM25256	Coriell
GM26107	Coriell
ESI-035	ESI BIO
HUES 8	Harvard Stem Cell Institute
HUES 9	Harvard Stem Cell Institute
HUES 53	Harvard Stem Cell Institute
HUES 64	Harvard Stem Cell Institute
NCRM4	NIH
NCRM5	NIH
ND1-4	NIH
CMT2A-1.1	WiCell
CMT2A-1.2	WiCell
CMT2A-2.1	WiCell
CMT2A-2.2	WiCell
CMT2A-3.1	WiCell
CMT2A-3.2	WiCell
JHU078i	WiCell
JHU198i	WiCell
MCW027i	WiCell
MCW032i	WiCell
WA01	WiCell
WA01 Oct4-GFP	WiCell
WA09	WiCell
WA09 Syn-GFP	WiCell
WA13	WiCell
WA14	WiCell
WA17	WiCell
WA26	WiCell

Table S1. Overview of cell lines cultured with CTST and experiments represented in this study
List of hESC and hiPSC lines that were robotically cultured over the last 5 years by the stem cell team at NCATS and used for various projects. To date, the listed cell lines have undergone robotic cell expansion to generate more than 3720 cryovials with ten million hESCs or hiPSCs per vial. The cell lines WA09 and LiPSC-GR1.1 were systematically characterized in this study as indicated.

Vessel	Surface Area Per Well (cm^2)	Total Vessel Surface Area (cm^2)	CompacT SelecT Capacity	Total Surface Area (cm^2)	Media Change Speed (min)	Media Changes Per Day	Manual Media Changes Per Shift (8h)
T175 Flask	175	175	90	15750	2	720	240
T75 Flask	75	75	90	6750	2	720	240
T175 Triple Flask	525	525	90	47250	2	720	240
6-Well Plate	9.5	57	190	10830	6	240	80
24-Well Plate	1.9	45.6	190	8664	6	240	80
96-Well Plate	0.32	30.72	280	8602	6	240	80
384-Well Plate	0.056	21.504	280	6021	6	240	80

Table S2: Comparing the efficiency of robotic versus manual cell culture
Automated versus manual cell culture features can be compared considering different plate formats, speed of media changes and number of possible media changes based on the scenario that automation allows non-stop 24 h cell culture work, whereas manual cell culture is performed during a typical 8 h workday. In addition, while manual cell culture is typically done in 6-well plates, the CTST system can handle various flask and plate formats listed here.

Table S3. Differentially expressed genes in manually versus robotically cultured cells
List of genes that were up- or downregulated in hiPSCs and hESCs after manual or robotic cell culture. Data are from n = 5573, 4835, 4485 or 3922 single cells obtained from n = 4 independent experiments using two independent cell lines for “hESC Manual”, “hiPSC Manual”, “hESC Auto” and “hiPSC Auto”, respectively. Single-cell RNA-seq data were analyzed in the Seurat R package. See also Figure 3 for more details. **See Supplemental Excel File Table S3.**

Table S4. Helios, TaqMan, Western blot, and Immunofluorescence reagents
A CyTOF antibody panel against 28 targets for pluripotency, DNA damage, apoptosis and stress-signaling pathways as used for the experiment shown in Figure 4. List of TaqMan probes used for RT-PCR analyses. List of antibodies used for western blot and immunofluorescence.
See Supplemental Excel File Table S4.

	Initial (Million)	Final (Million)	Scale-up per Plate or Flask (Million)						
Cell Type	**Cells/cm²**	**Cells/cm²**	**384-well**	**96-well**	**24-well**	**6-well**	**T75**	**T175**	**T175 Triple**
Ectoderm	0.10	0.90	19.4	26.65	41.04	51.30	67.50	157.50	472.50
Mesoderm	0.05	0.45	9.66	13.82	20.52	25.65	33.75	78.75	236.25
Endoderm	0.20	0.40	8.60	12.29	18.24	22.80	30.00	70.00	210.00
Hepatocytes	0.10	0.30	6.45	9.22	13.68	17.10	22.50	52.50	157.00
Cardiomyocytes	0.09	0.10	2.15	3.07	4.56	5.70	7.50	17.50	52.50
Neurons	0.05	0.43	9.30	13.21	19.61	24.51	32.25	75.25	225.75

Table S5. User-friendly scalable production of different cell types by CTST
Depending on experimental needs, various cell types can be derived from hPSCs and produced at large scale in different cell culture vessels.

Reference	Automated System	Culture Medium for hPSCs	Coating Substrate	Passaging Reagent	Differentiation	Automated Scalability	Chemically Defined	Analysis
Thomas et al., 2009	CompacT SelecT	MEF-Conditioned Medium	Matrigel	Trypsin	Manual Embryoid bodies Cardiomyocytes	Partial	No	Pluripotency markers Karyotype MEA
McLaren et al., 2013	CompacT SelecT	N/A	PLO-Laminin	Trypsin	Automated Lt-NES	Partial	N/A	Neural markers
Soares et al., 2014	CompacT SelecT	CDM-PVA	Porcine gelatin-MEF/FBS	Collagenase IV, Dispase	Manual Multi-linage	Partial	No	Pluripotency markers qPCR
Tristan et al., present study	CompacT SelecT	E8 Medium (chemically defined)	Recombinant Vitronectin (chemically defined)	EDTA (enzyme-free)	Automated Monolayer Multi-lineage Embryoid bodies Neurospheres Cortical Neurons Cardiomyocytes Hepatocytes Others (not shown in present study)	Full	Yes	Comparison manual vs. robotic Pluripotency markers Karyotype Scorecard/qPCR Bulk culture RNA-Seq Single-cell RNA-Seq Mass cytometry Metabolic analysis Robotic MEA Disease modeling High-throughput screening

Table S6. Overview and comparison of previous reports and the present study utilizing CTST
Note the various advantages of the present study as compared to previous reports including the use of chemically defined media, enzyme-free passaging and more extensive analysis and characterization of cells generated by automation.

SUPPLEMENTAL MOVIES

Movie S1: Robotic cell culture of hiPSCs using the CTST system

Movie shows a routine step during cell passaging when hiPSCs cultured in large flasks are detached and prepared for plating into new flasks. Full movie showing the various automated functions carried out under sterile conditions and mimicking the manual cell culture process is available here: https://youtu.be/-GSsTSO-WCM

SUPPLEMENTAL EXPERIMENTAL PROCEDURES

Automated and manual cell culture

All hESC and hiPSC lines (Table S1) were maintained under feeder-free conditions in E8 medium (ThermoFisher) and VTN-N-coated (ThermoFisher) microplates or T175 flasks. Cells were passaged using 0.5 mM EDTA in phosphate buffered saline (PBS) without calcium or magnesium (ThermoFisher) every 3-4 days. After passage cells were counted using the automated Vi-cell XR counter (Beckman) on the CTST platform and cells were plated at a density of 1.5×10^5 cells/cm^2 in E8 cell culture medium supplemented with the CEPT cocktail for the first 24 h (Chen et al., 2021). All karyotyping analysis were performed by Cell Line Genetics (Madison, WI). Cells were maintained in a humidified 5% CO_2 atmosphere at 37 °C. To optimize cell survival and cytoprotection during cell passaging of pluripotent and differentiated cells, we used the recently developed CEPT cocktail (Chen et al., 2021) consisting of 50 nM Chroman 1 (#HY-15392; MedChem Express), 5 μM Emricasan (#S7775; Selleckchem), Polyamine supplement (#P8483, 1:1000 dilution; Sigma-Aldrich) and 0.7 μM Trans-ISRIB (#5284; Tocris). All manual cell culture experiments were performed in parallel to automated cell culture and matched for cell passage number and density throughout the study.

Live-cell metabolic assays by using Seahorse XF Analyzer

hES/iPS cells were dissociated by using Accutase, counted and seeded at 15,000 cells per well and incubated for 24 hours at 37°C in 5% CO_2 atmosphere. On the day of measurement, media was changed to Seahorse assay media containing 1 mM pyruvate, 2 mM glutamine and 10 mM glucose supplemented with 400 ng/mL of Hoechst and incubated in a CO_2-free incubator for 1 hour. Cell number was obtained by imaging for Hoechst- or DAPI-positive nuclei in a Celigo Image Cytometer (Nexcelom) for data normalization. Mitochondrial metabolism (OCR) and glycolysis (ECAR) were analyzed with Seahorse Mito, Glycolysis and Phenotype Stress Test Kits (Agilent).

Multi-electrode array (MEA)

hES/iPSC-derived neurons were plated at a density of ~5 million neurons/cm^2 in complete media containing laminin (10 μg/mL, ThermoFisher) and Y-27632 (10 μM, Tocris). After confirming the superiority of the CEPT cocktail, we replaced Y-27632 by CEPT. Twenty-four hours post-plating, media was replaced with neuron maintenance media and 50% media exchange was performed every 2-3 day. Recordings were acquired day 7 and 14 post plating. iPSC-derived cardiomyocytes were plated at a density of ~63,000 cardiomyocytes/cm^2 in cardiomyocyte media using CEPT cocktail. Forty-eight hours post-plating media was replaced with cardiomyocyte maintenance media and complete media changes were performed every 2 days. For cardiomyocytes MEA plates were coated with 8 μL of fibronectin (50 μg/mL; Sigma) over the electrode recording area. For plating neuronal cells, MEA plates were coated with poly(ethyleneimine) (0.1%, Sigma) in borate buffer (pH 8.4).

Mass cytometry time-of-flight (CyTOF)

Human ES/iPS cells were dissociated into single cells with Accutase for 12 min at 37°C. After single cell dissociation, cells were then stained with 2.5 μM Cell-ID Cisplatin (201064, Fluidigm) in MaxPar PBS (201058, Fluidigm) to discern viable (negative) and non-viable cells (positive). Surface antibody staining was performed at RT for 30 min in MaxPar Cell Staining Buffer (201068, Fluidigm). The cells were then fixed with freshly prepared 1.6% formaldehyde (28906, Thermo-Fisher) solution in MaxPar PBS for 20 min. Permeabilization was performed at RT for 15 min using 25% Nuclear Antigen Staining Buffer Concentrate (S00111, Fluidigm) in Nuclear Antigen Staining Buffer Diluent (S00112, Fluidigm). Then the cells were stained with antibodies against intracellular targets in Nuclear Antigen Staining Perm (S00113, Fluidigm) at RT for 45 min.

To identify cellular events, the cells were stained with 250nM Iridium Intercalator (201192B, Fluidigm) in MaxPar Fix and Perm Buffer (201067, Fluidigm). The cells were loaded into the cytometer in Cell Acquisition Solution (201240, Fluidigm) supplemented with 10% EQ™ Four Element Calibration Beads (201078, Fluidigm) for signal normalization. The data acquisition was performed using Helios™, a CyTOF® mass cytometer system (Fluidigm). The acquired data was normalized based on EQ Four Element Calibration Beads signal using R/Shiny package “premessa” (https://github.com/ParkerICI/premessa). Beads were then excluded and dead cells, aggregates and non-cellular events were gated out. The single cellular events were retained and the data were analyzed using a modified CyTOF workflow (Robinson et al., 2017). A total of 200000 events were collected for each sample, including normalization beads. The

numbers of single live cells that passed the gate criteria were used for subsequent analysis were: WA09 auto 32889 cells, WA09 manual 11898 cells, LiPSC-GR1.1 auto 32857 cells, LiPSC-GR1.1 manual 19217 cells. To construct the UMAP plots, 8,000 cells were used from each sample. The panel of antibodies is provided in Table S4.

Flow cytometry analysis of cardiomyocytes

On day 24 of cardiomyocyte differentiation, cells were dissociated using the Cardiomyocyte Dissociation Kit (STEMCELL Technologies). Dissociated cells were resuspended in Intracellular Fixation and Permeabilization Buffer (ThermoFisher) and incubated for 15 min at RT. Cells were stained with primary antibodies against cardiac actin (Sigma, MABT823, 1:50) or IgG control (Millipore, CBL610, 1:100) were added and incubated for 1 h at RT, followed by FITC-conjugated goat anti-mouse secondary antibody (Millipore, cat# 12-506, 1:100) staining for 1 h at RT. Cells were washed twice with staining buffer and analyzed using a BD LSRFortessa Flow Cytometer (BD Biosciences).

Single-cell RNA library preparation and sequencing

Cells were dissociated by 10 min incubation with Accutase (Sigma) at 37 °C to obtain a single cell suspension, washed with PBS, pelleted and resuspended in PBS at a cell concentration of 1,000 cells per µL. GEMs were transferred to PCR 8-tube strips and GEM-reverse transcription was performed in a C1000 Touch Thermal Cycler (BioRad): 53 °C for 45 min, 85 °C for 5 min and held at 4 °C. GEMs were lysed in recovery buffer and single-stranded cDNA was cleaned up using silane DynaBeads (ThermoFisher). cDNA was amplified in a C1000 Touch Thermal Cycler (BioRad): 98°C for 3 min, cycled 12X: 98 °C for 15 sec, 67 °C for 20 sec, 72 °C for 1 min; 72 °C for 1 min and held at 4 °C. Amplified cDNA was cleaned up using the SPRIselect Reagent (Beckman Coulter). Post cDNA amplification QC and quantification was done using a High Sensitivity D5000 ScreenTape Assay (Agilent) on a 4200 TapeStation System (Agilent). Library Construction was done by fragmentation at 32 °C for 5 min, end repair and A-tailing at 65°C for 30 min. Post fragmentation, end repair and A-tailing double-sided size selection was done using the SPRIselect Reagent (Beckman Coulter). Adaptor ligation was done at 20°C for 15 min. Post ligation cleaned up using the SPRIselect Reagent (Beckman Coulter). Sample indexing was done using the i7 Sample Index Plate (Chromium) in a C1000 Touch Thermal Cycler (BioRad): cycled 10-12X: 98 °C for 45 sec, 98 °C for 20 sec, 54 °C for 30 sec, 72 °C for 20 sec; 72 °C for 1 min and held at 4 °C. Post sample index PCR double sided size selection done using the SPRIselect Reagent (Beckman Coulter). Post library construction quantification was done using a High Sensitivity D1000 ScreenTape Assay (Agilent) on a 4200 TapeStation System (Agilent). Sequencing libraries were quantified by qPCR using the KAPA library quantification kit for Illumina platforms (KAPA Biosystems) on a QuantStudio 12K Flex Real-Time PCR System (ThermoFisher). Libraries were loaded on an Illumina HiSeq 3000 using the following: 98bp Read1, 8bp i7 Index and 26bp Read2.

Analysis of single-cell RNA-seq

The Cellranger software package from 10X Genomics, Inc. (version 3.0.1) was used to process raw BCL files from single cell sequencing as follows. Pipeline details can be found at https://github.com/cemalley/Tristan_methods. This work used the computational resources of the NIH HPC Biowulf cluster (http://hpc.nih.gov). Demultiplexing and FASTQ generation were done with the mkfastq command, and the count command created gene expression matrices. Dense matrices were created with the mat2csv command. Embryonic stem cell and iPSC lines were analyzed in the Seurat R package (Seurat 2.3.4; R 3.5.2) (Stuart et al., 2019). The FindMarkers and FindAllMarkers functions were used to perform Wilcoxon rank sum tests of differential expression between samples or clusters. Cluster determination used the FindClusters function with default resolution parameter, which runs a shared nearest neighbor modularity optimization-based clustering algorithm. Expression dynamics due to cell cycle were regressed out using the CellCycleScoring function. See the code at https://github.com/cemalley/Tristan_methods for full details. Further data visualizations were made in R and with the ggplot2 package (3.1.0). Samples were checked for expression of markers of glycolysis, aerobic respiration, pluripotency, the peroxisome, the pentose phosphate shunt and the TCA cycle.

Automated and manual differentiation into embryonic germ layers

For endoderm differentiation, hES/iPS cells were plated at a density of 150,000 cells/cm^2 on VTN-coated T75 flasks in 15 mL of E8 media supplemented with CEPT cocktail and allowed to reach 50-60%

confluency. After reaching 50-60% confluency cell culture media was switched to TeSR-E8 Pre-Differentiation media for 24 h or until cells reached 70% confluency. Cells were single-cell dissociated by 10-15 min incubation with EDTA (0.5 mM, ThermoFisher) in phosphate buffered saline (PBS) without calcium or magnesium (ThermoFisher) at 37 °C and plated at a density of 210,000 cells/cm^2 onto VTN-coated T75 flasks in 15 of TeSR-E8 Pre-Differentiation media supplemented with CEPT cocktail. Twenty-four hours post plating cell culture media, flasks were rinsed with DMEM/F12 and media was replaced with 15 mL of Medium 1 (STEMdiff Definitive Endoderm Basal Medium with STEMdiff Definitive Endoderm Supplement A and STEMdiff Definitive Endoderm Supplement B). The next day cell culture media was exchanged with 15 mL Medium 2 (STEMdiff Definitive Endoderm Basal Medium with STEMdiff Definitive Endoderm Supplement B). On Days 3-5, cell culture media was changed with 15 mL Medium 2 (STEMdiff Definitive Endoderm Basal Medium with STEMdiff Definitive Endoderm Supplement B). Endoderm cells were analyzed on day 5.

For mesoderm differentiation on day 0 cells were plated at a density of 50,000 cells/cm^2 on VTN-coated T75 flasks in 15 mL of E8 media supplemented with CEPT cocktail and incubated for 24 h. On days 1-5 cell culture media was replaced with 22.5 mL of STEMdiff Mesoderm Induction Medium (STEMCELL Technologies). On day 5, mesoderm cells were analyzed.

For ectoderm differentiation cells were plated at a density of 50,000 cells/cm^2 on VTN-coated T75 flasks in 15 mL of E8 media supplemented with CEPT cocktail and allowed to reach 70% confluency. After reaching 70% confluency cell culture media was switched to E6 with 100 nM LDN-193189 and 2 µM A83-01. Media was changed daily for 6 days. On day 7, cells were ready to be assayed. For all differentiation protocols, cells were maintained in 5% CO_2 atmosphere at 37 °C and all media changes were done at 24 h intervals. All automated and manual differentiations were performed in parallel as mentioned above.

Automated neuronal differentiation

For neuronal differentiation, hESCs and hiPSCs by were single-cell dissociated by 10-15 min incubation in EDTA (0.5 mM, ThermoFisher) in phosphate buffered saline (PBS) without calcium or magnesium (ThermoFisher) at 37 °C and plated at a density of 50,000 cells/cm^2 onto VTN-coated T75 flasks in 15 mL of E8 media supplemented with CEPT cocktail. After reaching 70% confluency cell culture media was switched to E6 with 100 nM LDN-193189 and 2 µM A83-01. Cells were then given daily media changes for 6 days. On day 7, cells were single cell dissociated by 5 min incubation with Accutase, rinsed in PBS without calcium or magnesium and resuspended in E6 supplemented with CEPT cocktail and transferred into ultra-low attachment T175 flasks in 30 mL of media. After 24 h, formed neurospheres were allowed to settle and cell culture media was switched to DMEM/12 GlutaMAX (ThermoFisher) supplemented with BDNF (10 ng/mL, R&D Systems), GDNF (10 ng/mL, R&D Systems), N2 (ThermoFisher), B27 without Vitamin A (ThermoFisher), cyclic-AMP (50 µM, Tocris) and Ascorbic Acid (200 µM, Tocris) and maintained in suspension in ULA T-175 flasks. Media was changed every 2 days for two weeks. Cells were then transferred into T175 flasks coated with Geltrex (ThermoFisher) and maintained in DMEM/12 GlutaMAX supplemented with BDNF (10 ng/mL), GDNF (10 ng/mL), N2, B27 without Vitamin A, cyclic-AMP (50 µM, Tocris) and Ascorbic Acid (200 µM, Tocris) for 2 weeks. Thereafter, cells were ready to be assayed. Cells were maintained in a 5% CO_2 atmosphere at 37 °C and all media changes were done at 24 or 48 h intervals. All automated and manual differentiations were performed in parallel as mentioned above.

Automated and manual cardiomyocyte differentiation

hES/iPS cells were single-cell dissociated by 10-15 min incubation with EDTA (0.5 mM, ThermoFisher) in phosphate buffered saline (PBS) without calcium or magnesium (ThermoFisher) at 37°C and plated at a density of 150,000 cells/cm^2 onto matrigel-coated T75 flasks in 15 mL of E8 media supplemented with CEPT cocktail. Daily E8 media changes were done until cells reached 95% confluency. Once cells were 95% confluent (Day 0) cell culture media was exchanged with 15 mL of Cardiomyocyte Differentiation Medium A (STEMdiff Cardiomyocyte Differentiation Basal Media with Supplement A) with Matrigel (1:100, Corning). On day 2, cell culture media was exchanged with 15 ml of Cardiomyocyte Differentiation Medium B (STEMdiff Cardiomyocyte Differentiation Basal Media with Supplement B). On days 4 and 6, cell culture media was exchanged with 15 mL of Cardiomyocyte Differentiation Medium C (STEMdiff Cardiomyocyte Differentiation Basal Media with Supplement C). After day 8, cell culture medium was exchanged every 2 days with 15 mL Cardiomyocyte Maintenance Medium (STEMCELL Technologies). On day 30, cells were ready to be assayed. Cells were maintained in 5% CO_2 atmosphere at 37 °C. All automated and manual differentiations were performed in parallel as mentioned above.

Automated and manual hepatocyte differentiation
hESCs and iPSCs were single-cell dissociated by 5 min incubation in EDTA (0.5 mM, ThermoFisher) in phosphate buffered saline (PBS) without calcium or magnesium (ThermoFisher) at 37 °C and plated at a density of 10,000 cells/cm^2 onto Laminin 521 (62.5 µg/cm^2, Biolamina)-coated 384-well plates in 30 µL of E8 media supplemented with CEPT cocktail or Y-27632 (10 µM, Tocris). After 24 h, differentiation was initiated by daily media changes with 25 µL per well of RPMI 1640/HEPES (ThermoFisher) supplemented with PenStrep (ThermoFisher), NEAA (ThermoFisher), 2% B27 (ThermoFisher), bFGF (20 ng/mL, ThermoFisher), Activin A (50 ng/mL, ThermoFisher) and BMP4 (10 ng/mL, R&D Systems) for 2 days. On days 3-5, media was exchanged daily with 25 µL per well of RPMI 1640/HEPES supplemented with PenStrep, NEAA, 2% B27 and Activin A (50 ng/mL). On days 6-10, media was exchanged daily with 25 µL per well of RPMI 1640/HEPES supplemented with PenStrep, NEAA, 2% B27, bFGF (10 ng/mL) and BMP4 (10 ng/mL, R&D Systems). On days 11-15, media was exchanged daily with 25 µL per well using RPMI 1640/HEPES supplemented with PenStrep, NEAA, 2% B27 and HGF (20 ng/mL, Peprotech). On days 16-20, media was exchanged daily with 25 µL per well of HCM Bullet Kit medium (Lonza). On day 21 cells were ready to be assayed. Throughout all steps, cells were maintained in 5% CO_2 atmosphere at 37 °C and all media changes were done at 24 h intervals. All automated and manual differentiations were performed in parallel as mentioned above.

RT-qPCR
RNA was isolated from automated and manually differentiated hiPSC-derived hepatocyte cell cultures using the RNeasy Plus mini kit (Qiagen, 74136). To increase RNA yields from cardiomyocyte cultures the RNeasy Fibrous Tissue Mini Kit (Qiagen, 74704) was used. RNA was used to synthesize cDNA using the high-capacity RNA to cDNA (Applied Biosystems, 4387406). qPCR was done using the TaqMan Gene Expression Master Mix (Applied Biosystems, 4369016) in a QuantStudio 7 Real Time-PCR system. RPL13A or GAPDH were used as a house-keeping genes and for normalization. List of probes is provided in Table S4.

Immunocytochemistry
Cells were fixed with 4% paraformaldehyde (PFA) in PBS for 15 minutes, followed by permeabilization-blocking with 5% Donkey Serum and 0.1% Triton X-100 in PBS for 1 hour. Cells were then stained with primary antibodies overnight at 4 °C. All antibodies are listed in Table S4. Fluorescence images were taken with the Leica DMi8 microscope using appropriate filters.

Western blotting
Cells were harvested by scraping, pelleted, washed with PBS, flash frozen and stored at -20 °C until processed. Cells were lysed by sonication in RIPA buffer (ThermoFisher) supplemented with halt protease inhibitor cocktail (ThermoFisher). Western blots were performed using a Wes Capillary Western Blot analyzer (ProteinSimple) according to the manufacturer's recommendation. Protein quantification was done using the Compass software. Primary antibodies used are listed in Table S4.

Zika virus experiments
Vero (African green monkey kidney Vero 76) and wild-type Ugandan MR766 Zika Virus (ZIKV) were purchased from the American Type Culture Collection (ATCC; Manassas, VA). Vero cells were maintained in Dulbecco's Modified Eagle's Medium (DMEM) plus 10% Fetal Bovine Serum (FBS). ZIKV virus was amplified in Vero cells by inoculation with virus (multiplicity of infection [MOI] =1) for 3 h in a low volume of medium with 4% FBS (3 mL per T175 flask), with rocking every 15 min, before the addition of 37 mL of full growth medium. Virus-infected cells were incubated for 72 h before harvesting the virus-containing supernatant. Before storing virus aliquots at -80^{o}C, virus titer was determined by a viral plaque-forming assay in 4 × 10^5 cells in 6-well plates, as described (Baer and Kehn-Hall, 2014). Cells were seed into culture plates and incubated at 37 °C. For viral infection, the cells were seeded in culture plates and maintained in 5% CO_2 atmosphere at 37 °C overnight to allow cells to attach. The next day, ZIKV was added to the cells with a multiplicity of infection of 1.0. The cells were incubated with ZIKV for 24 h in 5% CO_2 atmosphere at 37 °C. Next, the inoculum was removed, cells were washed twice with PBS, followed by fixation and immunostaining.

Supplemental References

Chen, Y., Tristan, C.A., Chen, L., Jovanovic, V.M., Malley, C., Chu, P.H., Ryu, S., Deng, T., Ormanoglu, P., Tao, D., et al. (2021). A versatile polypharmacology platform promotes cytoprotection and viability of human pluripotent and differentiated cells. Nat. Methods *18*, 528-541.

Robinson, M.D., Nowicka, M., Krieg, C., Weber, L.M., Hartmann, F.J., Guglietta, S., Becher, B., and Levesque, M.P. (2017). CyTOF workflow: Differential discovery in high-throughput high-dimensional cytometry datasets. F1000Research *6*, 1–53.

Stuart, T., Butler, A., Hoffman, P., Hafemeister, C., Papalexi, E., Mauck, W.M., Hao, Y., Stoeckius, M., Smibert, P., and Satija, R. (2019). Comprehensive Integration of Single-Cell Data. Cell *177*, 1888-1902.e21.

Baer, A., and Kehn-Hall, K. (2014). Viral concentration determination through plaque assays: Using traditional and novel overlay systems. J. Vis. Exp. 1–10.